Order Number 9019853

On the role of atmospheric gravity waves in mesospheric dynamics

Makhlouf, Usama Butros, Ph.D.

University of Cincinnati, 1989

U·M·I
300 N. Zeeb Rd.
Ann Arbor, MI 48106

ON THE ROLE OF ATMOSPHERIC GRAVITY WAVES IN MESOSPHERIC DYNAMICS

A dissertation submitted to the

Division of Graduate Studies and Research
of the University of Cincinnati

in partial fulfillment of the
requirements for the degree of

DOCTOR OF PHILOSOPHY

in the Physics Department
of the College of Arts and Sciences

1989

by

Usama B. Makhlouf

B. S. , Birzeit University, 1981
M. S. , University of Cincinnati, 1983
M. S. , University of Cincinnati, 1984

UNIVERSITY OF CINCINNATI

November 28 19 89

I hereby recommend that the thesis prepared under my supervision by Usama Makhlouf

entitled ON THE ROLE OF ATMOSPHERIC GRAVITY WAVES IN MESOSPHERIC DYNAMICS

be accepted as fulfilling this part of the requirements for the degree of Doctor of Philosophy

Approved by:

Tai-Fu Tuan

Bernard Goodman

Dale R. Jones

James C. Russell

ABSTRACT

The effects of downward gravity wave reflection from atmospheric structure and horizontal winds; the geometry of the wave source and observation region; and the relative importance of the horizontal and vertical transport are being investigated for several different but often used gravity wave models. A quantitative study is also made on the relative importance of the purely gravitationally induced compression (G.I.C.) due to fluid particle altitude change and the actual wave compression which can occur at a fixed altitude in a gravity wave.

We have found that (1) for large scale gravity waves, the downward reflection from atmospheric structure is sufficiently large as to warrant the use of gravity wave models which propagate primarily along the horizontal directions and are stationary along the vertical direction; (2) for small and medium scale gravity waves the stationary model is required only for high altitude sources; (3) the horizontal wind have a profound effect on the downward reflection; (4) in the presence of waves the vertical density transport of the minor species which produce the airglow predominate over the horizontal and vertical velocity transport; (5) the results for density, pressure and temperature variations show that the G.I.C. effect predominate (>95%) for v/c < 20% where v is the horizontal phase velocity, and the relative importance depends strongly on frequency for wave periods less than 10 min. , but becomes totally independent

of the frequency for periods greater than 20 min. ; (6) the temperature measurements can be quickly converted to height variations wherever the G.I.C. effect predominates. In addition, the total kinetic energy density can be simply expressed in terms of height variation and, whenever the G.I.C. predominate, can be very easily obtained from temperature measurements.

In the memory of my Father.

Acknowledgements

I want first to express my sincere gratitude to Prof. T. F. Tuan for his guidance and ideas to complete this work and his help in publishing a major part of this dissertation. I would like also to express sincere appreciation to prof. D. Jones, Prof. J. Russel and Prof. B. Goodman for serving as committee members. Their helpful comments and suggestions have certainly enriched this work. Special thanks to prof. B. Goodman for his thorough remarks and comments .

Many thanks to the faculty, secretaries and graduate students of the Physics department. I am also grateful to the U.S. Airforce geophysics laboratory, the University of Cincinnati research council and the Graduate Student Association for their financial support. Special appreciation to my colleague, Dr. Jin-Jou Lin, Dr. Ding-Yi Wang, Mr. Joe Isler and Mr. He Fan, for their long term cooperation.

Finally, I would like to thank my family and relatives and acknowledge many individuals who helped me overcome many difficulties in the past years whether it was financial, moral or professional. Special thanks goes to Dr. Adnan Nayfeh, Dr. Ramzi Rehan, Dr. Henry Jackaman, Dr. Edward Sader, Dr. Taiseer Arouri, Mr. Duraid Daas, Ms. Diana Salman, Mr. Joseph Najjar, Mr. George Khader, Ms. Emily Makhlouf, Ms. Pat Dudsic, and also I like to extend my thanks to those who I forgot to mention their names unintentionally.

TABLE OF CONTENTS

Figure Captions

Figure 1

Profile of O_3 concentration in Km^{-3}.

Figure 1.1

Coordinate system in a horizontal plane.

Figures 2(a), 2(b) and 2(c)

Response of the O_3 profile ($\Delta N_d/N_o$) to gravity wave models (a), (b) and (c) with low horizontal phase velocity (33 m/sec) and a long period (2 hrs.). All three models start up in phase at $\omega t=0$.

Figures 3(a), 3(b) and 3(c)

The relative magnitude of the three terms in equation 3-3 .

Figures 4(a) and 4(b)

Plots of $\Delta N_d/N_o$ for models (a) and (b) at $\omega t=40^o$.

Figures 5(a) and 5(b)

Plots of $\Delta N_d/N_o$ for models (a) and (b) at $\omega t=80^o$.

Figures 6(a), 6(b) and 6(c)

Plots of $\Delta N_d/N_0$ for models (a), (b) and (c) at $\omega t=0$ and high phase velocity (260.9 m/sec).

Figures 7(a), 7(b) and 7(c)

The relative magnitude of the three terms in equation 3-3 , for the 260.9 m/sec horizontal phase velocity.

Figures 8(a) and 8(b)

Plots of $\Delta N_d/N_0$ in the presence of horizontal winds with the COSPAR-based gravity wave propagating along the wind direction in (a) and against the wind direction in (b).

Figures 9(a) and 9(b)

The relative magnitude of the three terms in equation (3-3) , for the cases in 8(a) and 8(b).

Figures 10(a) and 10(b)

Plots of $\Delta N_d/N_0$ for models (a) and (b) at $\omega t=40^o$ for the high horizontal phase velocity (260.9 m/sec) .

Figures 11(a) and 11(b)

Plots of $\Delta N_d/N_0$ for models (a) and (b) at $\omega t=80^o$ for the high horizontal phase velocity (260.9 m/sec) .

Figures 12(a), 12(b) and 12(c)

Plots of $\Delta N_d/N_o$ for models (a), (b) and (c) with a short period (6 min.) and a small horizontal phase velocity (58.03 m/sec) at $\omega t=0$.

Figures 13(a), 13(b) and 13(c)

The three terms in $\Delta N_d/N_o$ for the 58.03 m/sec horizontal phase velocity.

Figures 14(a) and 14(b)

$\Delta N_d/N_o$ for the 6 min. period, 58.03 m/sec horizontal phase velocity at $\omega t=40^o$.

Figures 15(a) and 15(b)

$\Delta N_d/N_o$ for the 6 min. period, 58.03 m/sec horizontal phase velocity at $\omega t=80^o$.

Figures 16(a), 16(b) and 16(c)

Plots of $\Delta N_d/N_o$ for models (a), (b) and (c) with a short period (6 min.) and an intermediate horizontal phase velocity (176.47 m/sec) at $\omega t=o$.

Figures 17(a), 17(b) and 17(c)

The three terms in $\Delta N_d/N_o$ for the 176.47 m/sec horizontal phase velocity.

Figures 18(a) and 18(b)

Plots of $\Delta N_d/N_o$ in the presence of horizontal winds with the COSPAR-based gravity wave propagating along the wind direction in (a) and against the wind direction in (b).

<u>**Figures 19(a) and 19(b)**</u>

Both show the three individual terms in $\Delta N_d/N_o$.

<u>**Figures 20(a) and 20(b)**</u>

$\Delta N_d/N_o$ for the 6 min. period, 176.47 m/sec horizontal phase velocity at $\omega t=40^o$.

<u>**Figures 21(a) and 21(b)**</u>

$\Delta N_d/N_o$ for the 6 min. period, 176.47 m/sec horizontal phase velocity at $\omega t=80^o$.

<u>**Figures 22(a) and 22(b)**</u>

Propagation of the direct and earth reflected waves in a uniform isothermal atmosphere for low altitude source 22(a) and a high altitude source 22(b) at asymptotic periods of 16, 30, 60, 90, 120 and 180 min. The rays show asymptotic group velocities. Regions of validity for models (a) and (b) are marked and the shaded regions show the height range where most mesospheric and lower thermospheric airglow observations are made.

<u>**Figure 23**</u>

Relative importance of the stationary wave model (model (b)) and the travelling wave model (model (a)) in a more realistic atmosphere which allows for heavy downward reflection from the troposphere and lower thermosphere.

Figure 24

Shows what happens to a gravity wave as it approaches a critical layer $\Omega=0$.

Figure 25

Shows the directions of wave propagation in which $v_{phx} < V_{ox}$.

Figure 26

A plot of the induced density variation due to gravitation (dashed-dotted line) and due to wave compression (solid line) as a function of v/c for wave periods > 20 min. .

Figures 27, 28, and 29

Plots of the induced density variation due to gravitation (dashed-dotted line) and due to wave compression (solid line) as a function of v/c for wave periods = 10, 6.4 and 5.2 min. respectively.

Figure 30

A plot of the induced temperature variation due to gravitation (dashed-dotted line) and due to wave compression (solid line) as a function of v/c for periods > 30 min. .

Figures 31, 32 and 33

Plots of the induced temperature variation due to gravitation (dashed-dotted line) and due to wave compression (solid line) as a function of v/c for wave periods = 10, 6.4 and 5.2 min. respectively.

Figure 34

A plot of the ratio of the kinetic energy density to the background pressure as a function of v/c for wave periods of 20, 10, 6.4 and 5.2 min. .

CHAPTER 1

INTRODUCTION

After Hines wrote his classic paper "Internal Atmospheric Gravity Waves at Ionospheric Heights" [Hines,1960], extensive work began to study the sources of Atmospheric Gravity Waves (AGW) and the role they play in the atmosphere.

AGW play an important role in various Airglow emissions especially in the middle atmosphere. Airglow emissions are being used as a remote sensing probe to study temperature profiles and fluctuations in the atmosphere, and to deduce the spatial and temporal variations of the concentration profiles of the various minor constituents. As the AGW propagate in the atmosphere, they affect the concentration profiles of various species and though give rise to fluctuations in the steady Airglow emissions.

Experimentally, several observational techniques with the aid of satellites, radars, lidars and rocket soundings etc. are used to measure temperature fluctuations in the atmosphere and to detect concentrations of minor constituents. Also wind velocities are sometimes measured using several radar techniques. All these data are studied and analyzed by scientists who try to model the atmosphere by establishing temperature , density , pressure and constituency profiles. In this modeling one tries to explain experimental data and to use it to trace back to the sources of the AGW and to predict their effects on the atmosphere.

Studies in the middle atmosphere takes into consideration both the chemistry and the dynamics. Chemistry is important due to the fact that the AGW influence the photochemistry by changing the concentrations of the chemically active constituents and also by changing the neutral temperatures and thus the temperature-dependent rate coefficients of certain chemical reactions. Dynamics, which is the topic of the following chapters, has to do with the mechanisms of propagation of the AGW in the atmosphere and their effects on the mesospheric optical emissions. Through these optical emissions, temperature fluctuations and kinetic energy densities are calculated, they are important components in studying stability and turbulence in the middle atmosphere.

Optical emissions of various wavelengths, generated by the decay of various atmospheric constituents, are affected by the propagation of the AGW in the atmosphere. To study this effect and compare it to experimental data, certain assumptions have to be made in order to solve the hydrodynamic equations. Each set of assumptions forms a model through which atmospheric gravity waves propagation is studied.

Chapter 2 gives a detailed look at four different models which are used to calculate various responses in density and temperature fluctuations of the minor constituents due to gravity waves . In comparing the four models, Ozone (O_3) was chosen, since it is a minor constituent with a layered structure in the mesosphere see Fig. (1), and, together with the Hydrogen, provides the primary mechanism for producing the Hydroxyl (OH) infrared emission, in which this particular emission has received considerable attention in recent airglow publications, (Hatfield et al 1981; Myrabo et al 1983; Myrabo and Deehr 1984; Schubert and Walterscheid 1985; Walterscheid et al 1986; Taylor and Hapgood 1988). The effects of the AGW on the Ozone layer using the four models is described in detail in Chapter 3.

The four models discussed in the next chapter are:

(a) Hines model , with an infinite, unbounded, isothermal atmosphere.

(b) Hines model with a rigid ground boundary condition.

(c) The COSPAR model of YU et al (1980), which is based on the COSPAR atmosphere (1972), and is a numerical model with a rigid ground boundary condition.

(d) The COSPAR model with wind profile.

Model (a), the simplest and most popular one has been used in a number of theoretical papers. (Porter et al 1974; Dudis and Reber 1976; Chiu and Ching 1978; Weinstock 1978; Schubert and Walterscheid 1985; Walterscheid et al 1986).

Model (b), which includes the rigid boundary condition, is complementary to model (a), and has not yet been studied in the literature. It has some convenient features and it is being used presently in studying the non-linear response of the AGW (Isler et al 1988). One nice feature of this model is that it is a standing wave model in the vertical direction, and when used to calculate the higher order responses in the atomic oxygen emission due to a linear gravity wave, by Isler et al (1988), a linear divergent term appeared, when the brightness was calculated by integration of the intensity of the emission using model (a), and was avoided when model(b) was used.

Model (c), is a numerical model based on a full wave treatment with reflection and transmission at all height levels and with a ground and upper boundary conditions. It was used by Hatfield (1981).

Model (d), is basically the COSPAR model (c), with the addition of a Zonal wind profile. This model has not been studied before.

Atmospheric Gravity Waves (AGW) are clearly to play an important role in the middle and upper atmosphere, and this arises the question about their origin. Chapter 4 investigates whether the geometry of the AGW sources is significant for the choice of a particular model to work with. By geometry of the source is meant whether the source is above or below the observation region. All these models have in fact been used in their monochromatic forms, this implies that the source is far away from the observation point. This is not a bad assumption since the waves, if for example one assumes a tropospheric source, have to travel hundreds or thousands of kilometers horizontally before reaching to the mesosphere, which is the observational region of interest between 80-100 km. A comparison between a low altitude and a high altitude source is done in Chapter 4 which leads to the conclusion that the best way to study the effects of the AGW is to use a linear combination of two models, one is a traveling wave and the other is a standing wave model.

Introducing background winds in a model, seems to be closer to reality and has a drastic effect on the results. Although several problems appear as a result of introducing the background winds, since wind shears caused by height variation of the background winds can cause gravity waves with certain phase velocity propagating upward to be reflected backward or get absorbed by the mean flow when it gets closer to a wind shear. A detailed look at what happens to the wave as it approaches a wind shear is discussed in Chapter 5 with an identification of the regions of phase velocities where heavy downward reflection or absorption can occur as a result of approaching a wind shear critical layer.

Chapter 6 discusses the variation in temperature, pressure and density due to the propagation of AGW in the middle atmosphere. These variations are induced by two mechanisms :

1- The Gravitationally Induced Compression (G.I.C.)
2- The Wave Induced Compression.

The two effects can be separated, and the results can be applied to the density, pressure and temperature variations, so as to find the relative importance of the (G.I.C.) compared to the wave compression in order to deduce the regions of phase velocities where the wave compression part can be ignored. In those regions, using only the (G.I.C.) enables us to express the total kinetic energy density in terms of height variations, which in turn can be obtained easily from temperature measurements.

Chapter 2

GRAVITY WAVE MODELS

2.1 Basic Hydrodynamics

The basic differential equations which govern the propagation of the Acoustic-Gravity waves in an isotropic, adiabatic and non-viscous atmosphere, are as follows:

$$\frac{D\rho}{Dt} = -\rho\vec{\nabla}.\vec{u} \tag{2-1}$$

$$\frac{D\vec{u}}{Dt} = -\frac{1}{\rho}\vec{\nabla}P - \vec{g} \tag{2-2}$$

$$\frac{DP}{Dt} = c^2\frac{D\rho}{Dt} \tag{2-3}$$

where

$$\frac{D}{Dt} = \frac{\partial}{\partial t} + \vec{u}.\vec{\nabla}$$

Assuming the background temperature and the horizontal wind velocity to be a function of the height z only, and using perturbation theory, let

$$P = P_o + \Delta P \tag{2-4}$$

$$\rho = \rho_o + \Delta\rho \tag{2-5}$$

$$u = V_{ox} + \Delta u \tag{2-6}$$

$$w = \Delta w \tag{2-7}$$

where

P_O : background pressure

ρ_o : background density

$\vec{g}$: acceleration due to gravity

V_{OX} : background wind along k_x-direction, see section 2.5

u,w : horizontal and vertical components of the velocity field, respectively.

ΔP : perturbed pressure

$\Delta\rho$: perturbed density

x,z : horizontal and vertical coordinates respectively, z increases upward.

c : the speed of sound

Assuming horizontal stratification, the monochromatic solution of Eq. (2-1) - (2-3) is of the form:

$$f(x,z,t) \propto f(z) \exp[\, i(\, \Omega t - k_X x)\,] \tag{2-8}$$

where

k_X : horizontal wave number

Ω : doppler shifted frequency

$\Omega = \omega - k_x V_{ox}$

ω : intrinsic wave frequency

Substituting Eqs. (2-4) - (2-8) into Eqs. (2-1) - (2-3) ,the linearized Hydrodynamic equations are obtained:

$$i\Omega(\Delta\rho) = -\rho_o \vec{\nabla}.\vec{u} - \vec{u}.\vec{\nabla}\rho_o \tag{2-9}$$

$$i\Omega(\Delta u) + (\Delta w)\frac{\partial V_{ox}}{\partial z} = \frac{1}{\rho_o} ik_x(\Delta P) \tag{2-10}$$

$$i\Omega(\Delta w) = \frac{1}{\rho_o}\left[-\frac{\partial(\Delta P)}{\partial z} - g(\Delta\rho)\right] \tag{2-11}$$

$$i\Omega(\Delta P) - g\rho_o(\Delta w) = c^2\left[i\Omega(\Delta\rho) + \vec{u}.\vec{\nabla}\rho_o\right] \tag{2-12}$$

2.2 (a) Hines Model

In model (a), which is the Hines model (1960). Hines assumed the atmosphere to be infinite, unbounded with a uniform background temperature, i.e. the temperature does not change with height. Also, Hines assumed that there is no background wind.

Under these assumptions the linearized Hydrodynamic Eqs. (2-9) - (2-12) the wave solutions for the horizontal and vertical velocities are obtained in the form (see Hines, 1960) :

$$\Delta u = \alpha(\omega k_x c^2)\left[k_z^2 + (\tfrac{2}{\gamma}-1)^2(\tfrac{1}{2H})^2\right]^{1/2} e^{i\phi} e^{z/2H} e^{i(\omega t - k_x x - k_z z)}$$

(2-13)

$$\Delta w = \alpha(\omega^3 - \omega k_x^2 c^2) e^{z/2H} e^{i(\omega t - k_x x - k_z z)}$$

where

$$\phi = \tan^{-1}\left(-\frac{2/\gamma - 1}{2k_z H}\right)$$

γ : ratio of specific heats, c_p/c_v

H : atmospheric scale heights

$$H = \frac{c^2}{\gamma g}$$

α : normalization constant

k_z : vertical wave vector

Notice that Δu and Δw differ by a phase angle ϕ . Since γ and H are constants within the Hines' background atmosphere, ϕ is determined solely by the vertical wave length from the wave vector k_z .

2.3 (b) Hines model with boundary

Model (b) , which is a semi-infinite isothermal atmosphere with no background wind ,$V_{ox} = 0$. It is similar to Hines model atmosphere assumptions except for the rigid ground boundary which is imposed in the model, i.e. , $\Delta w = 0$ at z=0 .

Under these assumptions, the Linearized Hydrodynamic Equations (2-9) - (2-12) can be combined into a one second order differential equation. For more details see (Yu et al , 1980; Tuan and Tadic , 1982).

$$\left[\frac{d^2}{dz^2} + k_z^2\right]\Psi = 0 \qquad \text{for } z>0 \qquad (2\text{-}14)$$

and Ψ satisfies the condition

$$\left.\frac{\partial \Psi}{\partial z}\right|_{z=0} = \eta \Psi|_{z=0} \qquad (2\text{-}15)$$

where

$$\Psi = \left(\frac{\omega}{\rho_o^{1/2}}\right)\Delta P$$

$$\eta = -\frac{1}{2}\left(\frac{g}{c^2} - \frac{\omega_b^2}{g}\right)$$

$\omega_b =$ Brunt-Vaisala frequency

The solution to equation (2-14) is given by

$$\Psi = \alpha\left[\left(k_z + i\eta\right)e^{-ik_z z} + \left(k_z - i\eta\right)e^{ik_z z}\right]$$

From this solution and equations (2-9) - (2-12) the wave solutions for the horizontal and vertical velocities are obtained in the forms :

$$\Delta u = \frac{\alpha k_x k_z}{\omega^2 \rho_s^{1/2}}\left[\cos k_z z + \frac{\eta}{k_z}\sin k_z z\right]e^{z/2H}e^{i(\omega t - k_x x)}$$

$$\Delta w = \frac{i\alpha}{\rho_s^{1/2}}\left(\sin k_z z\right)\frac{k_z^2 + \eta^2}{\omega_b^2 - \omega^2}e^{z/2H}e^{i(\omega t - k_x x)} \qquad (2\text{-}16)$$

where ρ_s : density at sea level

Clearly models (a) and (b) are different due to the fact that the ground boundary can produce a standing wave along the vertical direction. Both models, of course, produce travelling waves in the horizontal direction.

2.4 (c) The COSPAR model

Model (c), is a numerical model with the rigid ground boundary condition as in model (b). This model allows for the propagation of the discrete or guided and partially guided modes as well as for the continous or free modes.

This model incorporates realistic profiles for the temperature, mean molecular mass, ratio of specific heats and the acceleration due to gravity taken from the 1972 COSPAR models and the U.S. Standard Atmosphere (1965). The background atmosphere in this model is assumed to be stationary in the absence of waves, i.e. there is no background wind, $V_{ox} = 0$.

The linearized Hydrodynamic equations (2-9) - (2-12) are combined into two coupled Hydrodynamic equations after (Chimonas and Hines, 1986) given by:

$$\frac{\partial \Psi}{\partial z} - \eta \Psi = \frac{i}{\omega}\left(\omega_b^2 - \omega^2\right)\Phi$$

$$\frac{\partial \Phi}{\partial z} + \eta \Phi = i\omega\left[\frac{k_x^2}{\omega^2} - \frac{1}{c^2}\right]\Psi \qquad (2\text{-}17)$$

where

$$\Phi = \omega \rho_o^{1/2} \Delta w$$

The coupled equations (2-17) are numerically solved using the Runge-Kutta-Fehlberg method, (M.J. Marion, 1982) .

The model has to be modified above 120 km , where the thermal conduction and molecular viscosity gradually becomes significant.

2.5 (d) The COSPAR Model with Wind Profile

Model (d) is the same as model (c) except that mo the background wind is taken into consideration.

In considering the height varying background wind, the Zonal and Meridional wind profiles V_{oz} and V_{om} respectively, of Forbes (1982) are used which are based on the mean Zonal wind profile of Roble et al (1977); and only the case for 42^{o} N lattitude is considered.

Since the wind which is perpendicular to the direction of the wave propagation does not affect the wave itself, so only the effective wind acting on the wave has to be considered.

Assume that the angle between k_x and the East direction to be θ as in Fig. (1.1), the effective wind in the x-direction is :

$$V_{ox} = V_{oz} \cos\theta + V_{om} \sin\theta$$

Combining equations (2-9) - (2-12) with this effective wind in the horizontal direction , yield the two coupled Hydrodynamic equation after (Chimonas and Hines, 1986), as follows:

$$\frac{\partial \Psi}{\partial z} - \eta \Psi = \frac{i}{\Omega}\left(\omega_b^2 - \Omega^2\right)\Phi$$

(2-18)

$$\frac{\partial \Phi}{\partial z} + \left[\eta + \frac{k_X^2}{\Omega^2}\frac{\partial V_{ox}}{\partial z}\right]\Phi = i\Omega\left[\frac{k_X^2}{\Omega^2} - \frac{1}{C^2}\right]\Psi$$

By solving these coupled equations numerically, using the same technique as in model (c) , we obtain Δw and ΔP , and, through the horizontal momentum conservation, Δu can be obtained.

CHAPTER 3

DYNAMIC RESPONSE OF MINOR SPECIES TO AGW

3.1 Dynamical Density Fluctuation

The continuity equation for any species is given by:

$$\frac{\partial N}{\partial t} = Q - L - div(N\vec{u}) \qquad (3\text{-}1)$$

where

N : Concentration of the species

Q : Production rate

L : Loss rate

$\vec{u}$: Gravity wave velocity field

Using perturbation, and assuming horizontal stratification as in Chapter 2 . The first order linearized form of equation (3-1) is obtained in the form (Weinstock 1978; Hatfield et al 1981) :

$$\frac{\Delta N}{N_o} = -\frac{i}{\omega N_o}(\Delta Q - \Delta L) + \frac{k_x}{\omega}\Delta u + \frac{i}{\omega}\frac{\partial(\Delta w)}{\partial z} + \frac{i}{\omega}\frac{1}{N_o}\frac{\partial N_o}{\partial z}\Delta w \qquad (3\text{-}2)$$

where

ΔN : Fluctuation in the concentration produced by AGW

ΔQ : Fluctuation in the production rate

ΔL : Fluctuation in the loss rate

N_o : Background concentration

Neglecting Chemistry, and dealing with dynamic only, let's define ΔN_d as the density fluctuation from dynamics only to obtain:

$$\frac{\Delta N_d}{N_o} = \frac{k_x}{\omega}\Delta u + \frac{i}{\omega}\frac{\partial(\Delta w)}{\partial z} + \frac{i}{\omega}\frac{1}{N_o}\frac{\partial N_o}{\partial z}\Delta w \qquad (3\text{-}3)$$

Thus given any gravity wave model , one can calculate the dynamical fluctuation from (3-3).

The first term in (3-3) is the horizontal velocity transport, the second term is the vertical velocity transport, while the third term is the vertical density transport since it depends on the species density profile.

3.2 The Dominance of the Vertical Density Transport

In calculating the dynamical density fluctuation, one finds that the shape of the profile is a dominant term in the density fluctuation, i.e. , the third term in equation (3-3) is very important. To understand this lets consider two cases, the small and the large scale AGW.

Small scale AGW

For small scale gravity waves (small horizontal phase velocity and small horizontal and vertical wavelengths), k_x and k_z are both large. The horizontal and vertical velocity transport terms which are proportional to k_x and k_z (see Eq. 3-3) are therefore large relative to the vertical density transport which does not depend on these wave vectors. However, the first two transport terms for models (a) and (b) are 180° out of phase as shown below.

Table I shows the horizontal and vertical transport terms for both models (a) and (b) .

TABLE I

	1st term $\propto k_x \Delta u$	2nd term $\propto \frac{i\partial(\Delta w)}{\partial z}$
	horizontal velocity transport	vertical velocity transport
Hines model (a)	$e^{i\phi}$	$-(1+\frac{i}{2k_z H})$
Hines plus boundary (b)	$\cos k_z z + \frac{\eta}{k_z} \sin k_z z$	$-\cos k_z z - \frac{1}{2k_z H} \sin k_z z$

For small scale AGW, 2kz H >> 1 and η / k_z << 1 . So, for model (a) the horizontal and vertical velocity transport terms are proportional to 1 and -1 respectively, and by the same token the horizontal and vertical terms for model (b) are proportional to $\cos k_z z$ and $-\cos k_z z$, which lead to the 180^{o} out of phase.

Thus, in both models the two large velocity transport terms cancel leaving the remaining term involving the vertical density gradient predominant. For small scale gravity waves, the fluctuations of the atmospheric constituents depends therefore more strongly on the transport from the vertical density gradient.

Large scale AGW

For large scale atmospheric gravity waves k_x and k_z are both small and the two velocity transport terms for both models are both small, and the third term is again left to be predominant. Thus, one would expect the vertical density gradient term to dominate for both large scale and small scale gravity waves. Models (c) and (d) are both numerical models and cannot be placed in TABLE I. The third term is still dominant, but it is totally different for guided modes than for models (a) and (b).

3.3 A Comparison of the Four Models

Having discussed the general features, we can now apply all four gravity-wave models to the minor species O_3 to determine the difference in its response to AGW in the four models . There are in general two types of gravity waves: (1) those with long periods (> 25 min.) so that the complete spectrum of guided and free modes are independent of the frequency ω (Yu et al 1980); (2) those with short periods within the Brunt period (5-15 min.) for which the spectrum of the guided and free modes are dispersive and which are in general always fully guided for low altitude sources (Wang and Tuan 1986, 1988). We will now examine all these differences with specific examples.

To be specific, a two hour period is chosen, although our discussions would be the same for any long period (>25 min.) waves. The phases of the models are chosen so that at t=0 they all start with the same phase.

The vertically travelling wave model (a) and the vertically standing wave model (b) produce similar responses at t=0 for small scale gravity wave (horizontal phase velocity, v_{phx}=33 m/sec.), (see Fig. 2(a) and 2(b)) Model (c) produces a different response at higher altitudes due to the uneven background atmosphere at altitudes above 90 km where the vertical wavelength becomes shorter for the more realistic model. In general, especially at lower altitudes, there is a little difference between Model (c) (Fig. 2(c)) and the two isothermal models. This is because for the small scale waves there is far less vertical reflection.

As expected from the previous general analysis, the horizontal and vertical transport terms are large for all models and 180° out of phase (see Fig. 3(a) , (b) , (c)). In all cases the vertical density gradient then is left to dominate.

Consider now the time evolution of the wave; after one ninth of a cycle later ($\omega t=40°$), the responses to the travelling wave model (a) and the vertically stationary model (b) begin to differ but not by much (Fig. 4(a) and 4(b)) . The difference becomes drastic when we approach the quarter cycle ($\omega t=80^o$) ,(see Fig. 5(a) and (b)). This means that the heavy downward reflection from the base of the thermosphere can make a big difference in the response.

Model (d), which includes the background wind is only used in the comparison of large horizontal phase velocities due to the singularities which occur at small horizontal phase velocities.

For large scale gravity waves (v_{phx} =260.9 m/sec) and hence long vertical wavelengths (Figs. 6(a) and 6(b)) the horizontal and vertical velocity transport are small in magnitude, as expected from previous analysis and are too slowly varying along the vertical (due to long vertical wavelength) to affect the dominance of the vertical density transport (Figs. 7(a) and 7(b)). Thus the vertical density transport dominates for gravity waves of both small and large scale sizes. For model (c) , Figs. 6(c) and 7(c) shows a completely different response, which is not surprising, since at this height range the gravity wave is essentially evanescent for this model in contrast with the other models. Thus, for large scale gravity waves, the isothermal models given by model (a) & (b) are not valid. Figs. 8(a) and 8(b) shows the effects of wind on gravity waves with relatively high horizontal phase velocity. In Fig 8(a) the wave is propagating along the direction of the wind, while in Fig. 8(b) the wave is propagating in opposite direction to the wind. The results are totally different from the windless cases . Fig. 9(a) and 9(b) shows that the wind has a strong effect on all three transport terms. However, a comparison of

Fig. 9(a) and Fig. 8(a), Fig. 9(b) and Fig. 8(b) together with a comparison of Fig. 7(c) and Fig. 6(c) shows that for all these cases the vertical density transport term remains the dominating term.

Figs. 10(a), 10(b), 11(a) and 11(b) show the time evolution differences between models (a) and (b) for the high horizontal phase velocity 260.9 m/sec. The results show that, as in the low phase velocity case , the difference becomes only seriously significant for $\omega t=80^{o}$ or near the quarter of a cycle.

Figs. 12(a) , (b) , and (c) show the difference between models (a) , (b) , and (c) for a short period (6 min.) and a small horizontal phase velocity (58.03 m/sec), which is a fully guided mode. The guidance in this case is produced by the variation in the Brunt-period curve as a function of height (Wang and Tuan 1985, 1986, 1988), which unlike the usual structural guidance, is the only mechanism that can produce fully guided modes. Clearly the isothermal models cannot produce such guidance because the Brunt period does not vary with height . Whilst the COSPAR model (c) , shows a significant difference from models (a) and (b) at high altitudes. Figs. 13(a) , (b) and (c) again show the dominance of the vertical density transport in all three models. Figs. 14(a) , 14(b) ,15(a) and 15(b) shows the time evolution of the 6 min. , 58.03 m/sec horizontal phase velocity wave.

Figs. 16(a) , (b) and (c) is another comparison between models (a), (b) and (c) for a short period (6 min.) and a medium horizontal phase velocity (176.47 m/sec), which is again a fully guided mode. Figs. 17(a) , (b) and (c) again shows the dominance of the vertical density transport. A look at the effects of horizontal winds on the COSPAR model are shown in Figs. 18(a) and 18(b). A comparison of these two figures with Figs. 8(a) and 8(b) would seem to show that the wind effects are similar, i.e. when the wind is along the same direction as the wave propagation , and the doppler shift is toward the lower frequency and longer period end, the variation with height are much smaller and less pronounced This is because at the longer period end the waves are trapped over a much greater height range , whilst the opposite is true when the wave is propagating against the horizontal wind direction. Figs. 19(a) and 19(b) shows the effect of wind on all three transport terms. Figs. 20(a) , 20(b) , 21(a) and 21(b) again shows the time evolution of this 6 min. , medium horizontal phase velocity, (176.47 m/sec) wave.

CHAPTER 4

SOURCE GEOMETRY OF AGW

4.1 Potential Sources of AGW in the Atmosphere

Atmospheric Gravity Waves are considered as a coupling mechanism between various levels of the atmosphere. The AGW generated by various low altitude and high altitude sources , affect the chemistry and dynamics of the mesosphere. Several potential sources of the AGW had been proposed, such as the jet streams in the troposphere and stratosphere, thunderstorms in the troposphere, hurricanes , earthquakes , magnetic storm fluctuation in the intensity of the auroral electrojet which operates through two mechanisms, Joule Heating and Lorentz force, which generates large scale AGW, (Chimonas and Hines , 1970), There are also artificial wave sources such as bomb detonations.

However, it is very hard to link specific waveforms observed in the middle atmosphere with a definite source , since the wave travels hundreds or thousands of kilometers horizontally in the course of its upward propagation , before it's observed . Recently, there has been some success in linking certain wave-like structure with tropospheric weather systems. (Taylor and Hapgood, 1988 ; Taylor, 1989).

4.2 AGW Models and Source Location

Among the four Gravity Wave Models discussed in Chapter 2, none of these models contain an explicit source of the AGW. In this section, an investigation on whether the source geometry (i.e. , whether the source is below or above the observation region), gives any preference for a certain model, specifically, with a certain source geometry, whether to use a model with a ground boundary or without.

As mentioned before, all these models have been used largely in their monochromatic form. This in turn tacitly assumes that the observation point has to be sufficiently far away from the source to allow the waves to acquire their asymptotic periods. One can show (Francis , 1974), through using Green's Function and an explicit source, that, in a semi-infinite isothermal atmosphere with a rigid ground boundary , both the direct and earth reflected waves should form an upward travelling wave along the vertical direction above the altitude of the source in the far regions where the waves acquire their asymptotic periods, phase velocities and wave lengths. A travelling wave model in the vertical direction is then more appropriate to use, such as model (a). Below the source height and again in the far region the direct and earth reflected waves travel in opposite directions along the vertical and must produce a null point for the vertical velocity at the ground level. A standing wave in the vertical direction is then more appropriate for use. As an example, for field observations in the height range of 80 to 100 km, model (b) should be used for the high altitude sources (e.g. the auroral electrojet), whilst model (a) should be used for low altitude sources (e.g. the jet stream), see Figs. 22(a) and 22(b) .

In Fig. 22(a) we show the corresponding asymptotic wave propagation for a low altitude source (12 km). The field of observation is located in a height range in which model (a) is valid. Whilst, in Fig. 22(b) we show the gravity waves in the asymptotic region for a high altitude (120 km) source. The field of observation is within a height range in in which model (b) is valid. In general, when (b) is the more appropriate model, it is actually more realistic than (a) (Francis , 1974), since the ground reflected wave has a considerable longer distance to travel and has therefore more time to settle into its asymptotic conditions (i.e. more likely to be monochromatic).

In practice as already mentioned model (b) has far more wider applications than so far mentioned. For field observations below 100 km, which includes most of the observations we deal with here and in real atmosphere , there exists heavy downward reflection from two regions; the sudden sharp rise in the temperature above the base of the thermosphere and the heavy inhomogeneous dissipation at much higher altitudes. These two regions may be considered as providing implicit sources (as opposed to explicit sources we have so far been discussing). Thus, even if an explicit source is way below a field point so that model (a) should work , we would also need (b).

To estimate the relative importance of models (a) and (b) in the region below 100 km, we will primarily focus on horizontal phase velocities below 250 m/sec, which allows the reasonable approximation that the atmosphere is relatively uniform below 100 km and that downward reflection occurs only above this region. The wave solution below 100 km generated by a low altitude source is given by:

$$\Psi \propto e^{ik_z z} + R e^{-ik_z z}$$

$$= (1+R) e^{ik_z z} - 2iR\sin(k_z z) \qquad (4.1)$$

where

R: complex reflection coefficient with phase angle θ

$$|1+R| = \left(1+|R|^2 + 2|R|\cos\theta\right)^{1/2}$$

$$|2iR| = 2|R|$$

The first term in (4.1) is the upward travelling wave, model (a) while the second term is the vertical standing wave, model (b). Thus, we can in general split the solution generated by a source from below into a travelling wave and a stationary wave model. Within the limits of the approximation just mentioned, we can use the values of $|R|$ and θ from Francis' paper (1973 b) and obtain Fig. 23, which shows the relative amplitudes of model (a) and model (b). As can be seen in the Fig. 23, model (b) becomes more important than model (a) above 195 m/sec. Below this velocity both models are important, with (a) slightly favored.

CHAPTER 5

FILTRATION OF AGW BY TO WIND SHEARS

5.1 Windy case

As we have seen in Chapter 3 , the presence of the wind alters the response to gravity waves drastically in all cases. The individual transport terms are also affected. However, the vertical density transport remains the dominating effect. The critical layers from the horizontal winds, which often have very large velocity gradients along the vertical direction, can produce heavy downward reflection and thus may invalidate the use of model (a) for certain propagation directions.

5.2 The Critical layer due to Horizontal Wind

The critical layer, is the layer where the doppler shifted frequency $\Omega \rightarrow 0$. The doppler shifted frequency is given by:

$$\Omega = \omega\left(1 - \frac{V_{ox}}{v_{phx}}\right)$$

and, if the horizontal phase velocity of the wave in a layer is equal to the horizontal wind velocity , then in that layer the doppler shifted frequency goes to 0. Fig. 24 shows what happens to a gravity wave when it rises to a height level where $\Omega = 0$. The figure shows numerical calculations done at half-kilometer intervals. We have to choose the relatively slowly varying zonal wind profile at lower altitudes so that the calculations are numerically feasible. The critical layer is analogous to an infinite quantum potential barrier through which penetration is impossible. Consider what happens to a wave packet propagating upwards, theoretically the wave packet will never reach the critical layer in a finite time, because the group velocity approaches zero as the wave packet approaches the critical layer, which means that the atmospheric wave is either reflected or absorbed.

Currently, we are studying the reflection and absorption of the wave as it approaches a wind critical layer, in order to determine under what conditions the wave is reflected and under what conditions it will be absorbed.

In Fig. 25, the shaded regions shows, those directions of the wave propagation of waves with horizontal phase velocity less than the horizontal wind velocity, inwhich the wave is absorbed or reflected due to the wind critical layer. Three horizontal phase velocities are used, v_{phx} = 20 m/sec, 45 m/sec and 70 m/sec are chosen. Thus, within those regions, there is heavy downward reflection. The wind speeds can rise up at 20 m/sec pr km, a drastic change. Over a vertical distance of 3-4 km the wind speed become greater than the horizontal phase velocity and the solution to the hydrodynamic equation vanishes. In the unshaded regions mainly in the West directions, the waves do not face a critical layer and so the propagate freely to the upper atmosphere without being reflected or absorbed by the wind shear. This is because the horizontal winds that were used in plotting Fig. 25 shows that the winter wind velocity is higher towards the east direction, which could change seasonally. i.e. in the summer.

CHAPTER 6

FLUCTUATION MECHANISMS IN HYDRODYNAMIC VARIABLES DUE TO AGW

6.1 Gravitational versus Wave Compression

Several observational techniques have revealed spectacular wave-like structures in the Mesosphere and the Ionosphere. Photographs of Noctilucent clouds at a height of about 80 km, shows wave-like structures (Witt,1962). Hydroxyl (OH) airglow observation, which are used as a remote sensing mechanism to measure temperature variations in the Mesosphere, have shown images of wave-like structures in the OH emission intensity (see e.g. Peterson and Kieffaber, 1973; Moreels and Herse, 1977; Crawford et al, 1978; Peterson, 1979; Armstrong, 1982; Taylor, 1986; Taylor et al, 1987).

Theoretical studies have revealed that such wave-like structures are a result of AGW propagating through the emission layer (Francis, 1975; Fredrick, 1979; Hatfield et al, 1981), which in turn give rise to variation in the temperature, pressure and density. The variations are in general due to two mechanisms . One is the gravitationally induced compression (G.I.C.), which is an adiabatic expansion and compression process caused by the altitude change of a fluid parcel, while the other is the wave compression which occurs at a fixed altitude by the propagating wave.

The two mechanisms can be separated, and the regions of dominance of one over the other is investigated . If, for certain types of AGW, the G.I.C. effect can cause most of the fluctuations, so that we can neglect the wave compression, then very simple formulas can be developed to calculate the density, pressure and temperature fluctuations, as well as to make quick estimates of the gravity wave parameters.

6.2 G.I.C. Mechanism

The G.I.C. mechanism is an adiabatic process of expansion and compression, which takes place when a parcel of air is displaced by a vertical distance , h , in a hydrostatic atmosphere. At every instance in the vertical motion the pressures of the parcel and of the environment for a given level are assumed to be equal. The adiabatic assumption is reasonable, since the heat conduction processes in the atmosphere (turbulent diffusion, radiation, molecular conduction) are in general slow compared to convective movements.

When the parcel of air is displaced by h, its density is changed by $\Delta\rho_a$. This density change is produced by two changes:

1- Change in the background pressure, ΔP, where

$$\Delta P = \frac{\partial P_o}{\partial z} h = c^2 \Delta \rho_s$$

$\Delta\rho_s$: density variation due to change in background pressure.

2- Change in the background density, $\Delta\rho_o$, where

$$\Delta\rho_o = \frac{\partial\rho_o}{\partial z} h$$

Assuming a uniform isothermal background atmosphere with scale height H, one can calculate the net density change ratio to the background density as follows:

$$\frac{\Delta\rho_a}{\rho_o} = \frac{\Delta\rho_s}{\rho_o} - \frac{\Delta\rho_o}{\rho_o}$$

$$= \frac{1}{c^2\rho_o}\frac{\partial P_o}{\partial z} h - \frac{1}{\rho_o}\frac{\partial\rho_o}{\partial z} h$$

$$= -\frac{1}{\gamma H} h + \frac{h}{H}$$

where we used the Hydrostatic Equation : $\frac{\partial P_o}{\partial z} = -\rho_o g$

$$\therefore \qquad \frac{\Delta\rho_a}{\rho_o} = \left(\frac{\gamma - 1}{\gamma}\right)\frac{h}{H} \qquad (6.1)$$

where

$$\frac{1}{H}=-\frac{1}{\rho_o}\frac{\partial\rho_o}{\partial z}$$

6.3 A Comparison of the G.I.C. and the Wave Compression

In a Gravity Wave with angular frequency ω , the vertical displacement h can be written up to the first order as:

$h=w/i\omega$ where w is the vertical velocity field

Using the polarization relation of Hines' (1960) for $\Delta\rho/\rho_o$, one can show that up to the first order (see Appendix I):

$$\frac{\Delta\rho}{\rho_o}=\left(\frac{\gamma-1}{\gamma}\right)\frac{h}{H}+\left(\frac{v}{c}\right)^2\left(\frac{u}{v}\right)$$

$$=\frac{\Delta\rho_a}{\rho_o}+\frac{\Delta\rho_c}{\rho_o} \qquad (6.2)$$

where

u : horizontal field velocity

v : horizontal phase velocity

$\Delta\rho_c/\rho_o = (v/c)^2\ (u/v)$ = density fluctuation due to wave compression.

From equation (6.2), the G.I.C. term $\Delta\rho_a/\rho_o \rightarrow 0$ as $g \rightarrow 0$ since $H = c^2/\gamma g$. This implies that the only term left in equation (6.2) is the wave compression term $\Delta\rho_c/\rho_o$.

So for $g \rightarrow 0$, we obtain:

$$\left|\frac{\Delta\rho}{\rho_o}\right| \xrightarrow[g\rightarrow 0]{} \left|\frac{\Delta\rho_c}{\rho_o}\right| = \left|\frac{u\mathrm{v}}{c^2}\right|$$

and

$$\left|\frac{u\mathrm{v}}{c^2}\right| = \frac{(\mathrm{v}/c)}{\left[\left(\frac{\mathrm{v}}{c}\right)^2 - 1\right]^{1/2}} \frac{\omega}{c} |h| \tag{6.3}$$

For a derivation of equation (6.3), consult with Appendix IV.

At interest here is the relative importance of the G.I.C. $(\Delta\rho_a/\rho_o)$ as compared to the wave compression $(\Delta\rho_c/\rho_o)$. As one can see from equation (6.2), both the G.I.C. and the wave compression depends on (v/c) implicitly through h and u, and in order to remain well below the Lindzen (1981) criteria for gravity waves saturation, one should choose $|u| < \mathrm{v}$ (see Fritts,1984).

In general, since both $\Delta\rho_a$ and $\Delta\rho_c$ are complex quantities with different phases, considerable interference occurs between the two terms and, only if one has a magnitude of at least 4 to 5 times greater than the other, can one then neglect the smaller of the two.

To make quantitative comparison between $\Delta\rho_a$ and $\Delta\rho_c$, a plot of $|\Delta\rho_a|/|\Delta\rho|$ and $|\Delta\rho_c|/|\Delta\rho|$ as a function (v/c) is done.

In general, for any k_z , we have:

$$\left|\frac{\Delta\rho_a}{\Delta\rho}\right| = \frac{\frac{\gamma-1}{\gamma}\left(\frac{c^2}{v^2}-1\right)}{H\left\{(\mathrm{Re}(k_z))^2+\left[\frac{\gamma-1}{\gamma H}\left(\frac{c^2}{v^2}-1\right)+\eta+\mathrm{Im}(k_z)\right]^2\right\}^{1/2}}$$

$$\left|\frac{\Delta\rho_c}{\Delta\rho}\right| = \left\{\frac{(\mathrm{Re}(k_z))^2+(\eta+\mathrm{Im}(k_z))^2}{(\mathrm{Re}(k_z))^2+\left[\frac{\gamma-1}{\gamma H}\left(\frac{c^2}{v^2}-1\right)+\eta+\mathrm{Im}(k_z)\right]^2}\right\}^{1/2} \tag{6.4}$$

For the case when $k_z^2 > 0$, (see Appendix II) that:

$$\left|\frac{\Delta\rho_a}{\Delta\rho}\right| = \left[\frac{(\gamma-1)[1-(v/c)^2]}{(\gamma-1)-(\omega/\omega_b)^2(v/c)^2}\right]^{1/2} \tag{6.5}$$

$$\left|\frac{\Delta\rho_c}{\Delta\rho}\right| = \left[\frac{1-(\omega/\omega_b)^2}{(\gamma-1)-(\omega/\omega_b)^2(v/c)^2}\right]^{1/2}\left(\frac{v}{c}\right) \tag{6.6}$$

Thus, in general $|\Delta\rho_a|/|\Delta\rho|$ begins with the value unity (i.e. density variations are due entirely to G.I.C. compression) at v/c=0 , while $|\Delta\rho_c|/|\Delta\rho|$ begins at zero (i.e. no wave compression). As can be seen from equations (6.5) and (6.6) , when v/c increases, the behavior of $|\Delta\rho_a|/|\Delta\rho|$ and $|\Delta\rho_c|/|\Delta\rho|$ depend entirely on ω/ω_b for any value of v/c.

For long period gravity waves where $\omega \ll \omega_b$, we may neglect the terms involving ω/ω_b for both $|\Delta\rho_a|/|\Delta\rho|$ and $|\Delta\rho_c|/|\Delta\rho|$. So for long periods we can write:

$$\left|\frac{\Delta\rho_a}{\Delta\rho}\right| \approx \left\{1-\left(\frac{v}{c}\right)^2\right\}^{1/2} \tag{6.7}$$

$$\left|\frac{\Delta\rho_c}{\Delta\rho}\right| \approx \left(\frac{1}{\gamma-1}\right)^{1/2}\left(\frac{v}{c}\right) \tag{6.8}$$

As can be seen from equations (6.7) and (6.8) $|\Delta\rho_a|/|\Delta\rho|$ drops from unity as v/c increases, while $|\Delta\rho_c|/|\Delta\rho|$ increases linearly with v/c.

Fig. 26 shows this behavior for long period gravity waves $\tau>20$ min. Actually, there is little variation with period from 20 minutes on up and a plot for $\tau=120$ min. falls exactly on top of the corresponding curves for 20 minutes . Both curves are plotted from equations (6.5) and (6.6), but there would have been no difference if we had used equations (6.7) and (6.8). For $\tau=10$ min. , (Fig. 27) , $|\Delta\rho_c|/|\Delta\rho|$ begins to deviate from a straight line but only slightly, while $|\Delta\rho_a|/|\Delta\rho|$ drops somewhat less as v/c increases showing an increase in the importance of the G.I.C. relative to the wave compression for a given phase velocity. Furthermore, the crossover between the G.I.C. and the wave compression remains fairly constant at between v/c $\sim$ 55% to 60% . In general, for AGW with frequencies in this range (i.e. , τ =10 min.) , if we use the approximate criteria that $|\Delta\rho_a|/|\Delta\rho_c|$ has to be greater than a factor of 5 , then v/c has to be less than 15%, or the horizontal phase velocity has to be less than 45 m/sec. This covers a fairly large range and includes most of the observed mid-altitude small scale gravity waves from airglow data.

The vertical thin line indicates the position where $k_z^2 = 0$. It is easy to show from the Hines' dispersion formula that $k_z^2 = 0$ corresponds to :

$$\frac{v}{c} = \left(\frac{\omega_b^2 - \omega^2}{\omega_a^2 - \omega^2} \right)^{1/2} \tag{6.9}$$

To the left of this vertical line $k_z^2 > 0$ and the gravity waves may propagate freely. To its right $k_z^2 < 0$ and the gravity waves are evanescent in the vertical direction, although it still propagates along k_x . The dotted lines represent the evanescent region. At v/c = 1 , we have the Lamb mode for which there is no vertical motion and variations in density are caused entirely by wave compression, an exact reversal of what happens at v/c = 0 . The same reversal occurs in all figures.

As $\tau \to \tau_b$, (τ_b is the Brunt period), both $|\Delta\rho_a|/|\Delta\rho|$ and $|\Delta\rho_c|/|\Delta\rho|$ increases with v/c, (see Figs. 28 and 29) in such a way that the G.I.C. compression continues to dominate over a much greater range of horizontal velocities. In fact, in Fig. 29 where τ=5.2 min., the G.I.C. continues to dominate all the way to the vertical line ($k_z^2 = 0$), where v/c ~ 42% corresponding to a horizontal phase velocity well over 120 m/sec; a strictly medium-scale gravity wave (Francis, 1975). Thus, as the gravity wave period approaches the Brunt period, the G.I.C. dominates over a larger range of v and hence a larger range of wavelengths.

The pressure variation can be easily shown to be the same as $\Delta\rho_c$. By using the linearized momentum conservation equation, it can be shown that, for monochromatic waves,

$$\Delta P = \mathrm{v}\rho_o u$$

or

$$\frac{\Delta P}{P_o} = \frac{\gamma \mathrm{v} u}{c^2}$$

so

$$\frac{|\Delta P|}{c^2|\Delta\rho|} = \frac{|\Delta\rho_c|}{|\Delta\rho|} \qquad (6.10)$$

From Figs. 26-29, one can see that there is little pressure variation produced by the wave compression for small scale gravity waves. Only as the scale size of the gravity wave increases does it become important. Thus, for small scale gravity waves (v < 45 m/sec), the pressure variations are relatively insignificant.

6.4 Temperature Fluctuations

The temperature variations may be easily obtained from the linearized perfect gas law given by:

$$\frac{\Delta T}{T_o} = \frac{\Delta P}{P_o} - \frac{\Delta \rho}{\rho_o} \tag{6.11}$$

Using equations (6.2) and (6.10), we obtain,

$$\frac{\Delta T}{T_o} = (\gamma - 1)\left(\frac{vu}{c^2}\right) - \frac{\Delta \rho_a}{\rho_o} \tag{6.12}$$

Thus for small scale gravity waves (v << c),

$$\frac{\Delta T}{T_o} = -\frac{\Delta \rho_a}{\rho_o} = -\frac{(\gamma - 1)h}{\gamma H} \tag{6.13}$$

From equation (6.13), one can see that the temperature variation is opposite in phase to the gravitationally induced density compression. Let's define

$$\frac{\Delta T}{T_o} = \frac{\Delta T_a}{T_o} + \frac{\Delta T_c}{T_o}$$

where (6.14)

$$\frac{\Delta T_a}{T_o} = -\frac{\Delta \rho_a}{\rho_o} \quad ; \quad \frac{\Delta T_c}{T_o} = (\gamma - 1)\frac{uv}{c^2}$$

Again as in equations (6.5) and (6.6) it is possible to show that for $k_z^2 > 0$, (see Appendix III),

$$\left|\frac{\Delta T_a}{\Delta T}\right| = \left[\frac{1-(v/c)^2}{1-(\gamma-1)(\omega/\omega_b)^2(v/c)^2}\right]^{1/2} \tag{6.15}$$

$$\left|\frac{\Delta T_c}{\Delta T}\right| = \left[\frac{(\gamma-1)\left(1-(\omega/\omega_b)^2\right)}{1-(\gamma-1)(\omega/\omega_b)^2(v/c)^2}\right]^{1/2}\left(\frac{v}{c}\right) \tag{6.16}$$

Thus, once again, for v/c =0 , $|\Delta T_a|/|\Delta T| = 1$ and $|\Delta T_c|/|\Delta T| = 0$, and that in the low phase velocity limit (small scale gravity waves), the temperature variation is caused entirely by the adiabatic expansion and compression of an air parcel oscillating in the vertical direction (G.I.C.) . For long period gravity waves ($\omega << \omega_b$) , equations (6.15) and (6.16) can be simplified to:

$$\left|\frac{\Delta T_a}{\Delta T}\right| \approx \left[1-\left(\frac{v}{c}\right)^2\right]^{1/2} \tag{6.17}$$

$$\left|\frac{\Delta T_c}{\Delta T}\right| \approx (\gamma-1)^{1/2}\left(\frac{v}{c}\right) \tag{6.18}$$

Comparing equations (6.17) and (6.18) with equations (6.7) and (6.8), one can see that for long period gravity waves $|\Delta T_a|/|\Delta T|$ behaves the same way as $|\Delta\rho_a|/|\Delta\rho|$ in (6.7), whilst $|\Delta T_c|/|\Delta T|$ has a far more gradual slope than $|\Delta\rho_c|/|\Delta\rho|$. Thus, for temperature variations, the G.I.C. effect predominates over a greater range of phase velocities.

All this can be seen in Fig.30, which shows the behavior of $|\Delta T_a|/|\Delta T|$ and $|\Delta T_c|/|\Delta T|$ for gravity waves from 30 min. and up. Once again, a plot of both curves at $\tau = 120$ min. can be exactly superimposed over the curves for $\tau = 30$ min. . This is similar to the behavior of the curve of density variations (Fig. 26), which has a lower limit at $\tau = 20$ min. Again, for $\tau > 30$ min. there is no significant difference between equations (6.15), (6.16), (6.17) and (6.18) .

Figs. 31, 32 and 33 show the behavior of the temperature variations for $\tau = 10$, 6.4 and 5.2 min. respectively. The big difference between these temperature variations and the density variations given by Figs. 27, 28 and 29, is that for the temperature the effect of the G.I.C. is even much more important than the wave compression effect. For instance, at $\tau = 6.4$ min. , the wave compression effect overtakes the G.I.C. effect at v/c = 0.72 for the density variation, whereas the G.I.C. effect remains predominant in the corresponding temperature variation all the way to the vertical line ($k_z^2 = 0$). For both, however, the G.I.C. effect dominates all the way in the propagating region when $\tau = 5.2$ min. , approaching the Brunt period.

The dotted curves in all the Figures on the right hand side of the vertical line correspond to the evanescent waves with purely imaginary k_z . In this region one can no longer use the relatively simple expressions given by (6.15), (6.16), (6.17) and (6.18) , which were derived for real k_z . Instead one has to work with the general polarization relations given by Hines (1960).

From the above discussions, it is clear that comparatively small scale gravity waves with horizontal phase velocities less than 45 m/sec can be considered to be purely under the influence of the G.I.C. . This will allow us to make simple conversions from the measurement of temperature fluctuations to height fluctuations. Thus,

$$\left|\frac{\Delta T}{T_o}\right| \approx \left|\frac{\Delta T_a}{T_o}\right| = \frac{(\gamma-1)}{\gamma}\frac{|h|}{H} \qquad (6.19)$$

So, using the usual values for γ, H and T_O , we obtain the approximate conversion that a 10^o variation in temperature corresponds approximately to a height variation of 1 km. at 90-100 km. altitude.

6.5 Time-Averaged Kinetic Energy Density

The time-averaged kinetic energy density, K.E. , is given by :

$$K.E. = \frac{1}{4}\rho_o\left(|u|^2 + |w|^2\right) \qquad (6.20)$$

Using the polarization relations and Hines' dispersion relation, one can show (see Appendix IV) that:

$$K.E. = \frac{1}{4}\rho_o \omega_b^2 |h|^2 \left[\frac{1-(\omega/\omega_b)^2 (v/c)^2}{1-(v/c)^2} \right] \qquad (6.21)$$

For large scale gravity waves, where $v \to c$, the denominator in equation (6.21) can be much less than the numerator. This is especially true for long period gravity waves. Thus, the K.E. can be much greater than $\frac{1}{4}\rho_o \omega_b^2 |h|^2$. On the other hand, for small scale gravity waves ($v \ll c$), the K.E. is very accurately given by :

$$K.E. = \frac{1}{4}\rho_o \omega_b^2 |h|^2 \qquad (6.22)$$

It is interesting to note that equation (6.22) is true irrespective of the frequency of the small scale gravity waves. Since (6.22) is also the K.E. for the natural Brunt oscillation of a parcel of air, we may conclude that the total K.E. of the small scale gravity waves at any frequency is equivalent to the natural vertical atmospheric oscillations with the same vertical displacement. Here, the G.I.C. approximation for the density, pressure and temperature variations are also good. Using equations (6.19) and substituting it in equation (6.22) we get:

$$\frac{K.E.}{P_o} = \frac{1}{4}\left(\frac{\gamma}{\gamma-1}\right)\left|\frac{\Delta T_a}{T_o}\right|^2 \approx \frac{1}{4}\left(\frac{\gamma}{\gamma-1}\right)\left|\frac{\Delta T}{T_o}\right|^2 = 0.875\left|\frac{\Delta T}{T_o}\right|^2 \qquad (6.23)$$

where

P_o : background pressure energy.

Thus, a measurement of the rotational temperature variation can immediately yield the total kinetic energy density at any frequency for small scale gravity wave. In fact, (6.21) shows that the K.E. depends strongly on the frequency only for large scale gravity waves where $v \rightarrow c$.

6.6 Applications

To specifically apply the above analyses, three sets of observed data are chosen. Two sets of data involve gravity wave parameters well within the limits for the validity of the purely G.I.C. , while the other set is with parameters above the borderline.

The first set were data taken from Taylor and Hapgood (1988). The observed data include a gravity wave with a horizontal phase velocity of v = 21.7 m/sec, a horizontal wavelength of λ_x = 26 km, and a period τ = 20 min.

Using: g = 9.8 m/sec^2

H = 6.56 km

$\gamma = 1.4$

τ_b = 5.1 min. (the Brunt period)

c = 300 m/sec (the speed of sound)

Substituting these values in equation (6.12), with the help of Hines polarization and dispersion relations, one obtains:

$$\left|\frac{\Delta T}{T_o}\right| = 4.364x10^{-2}|h| \qquad (6.24)$$

where |h| is expressed in km. Using the G.I.C approximation, one obtains:

$$\left|\frac{\Delta T_a}{T_o}\right| = \frac{\gamma - 1}{\gamma}\frac{|h|}{H} = 4.355x10^{-2}|h| \qquad (6.25)$$

The error from using (6.25) is only 0.2% .

The second set were taken by Clairemidi, Hersh and Moreels (1985). They measured gravity waves with horizontal velocity v=15.6 m/sec and a period of 48 min. The full temperature fluctuation without approximation is given by:

$$\left|\frac{\Delta T}{T_o}\right| = 4.36x10^{-2}|h| \qquad (6.26)$$

Compared with the G.I.C. approximation given by (6.25), gives an error of the order of 0.1%.

The third set of data were taken by Witt (1962). The gravity wave observed had v = 75 m/sec, and λ_x = 50 km and the rest of the parameters are the same as the first data set. One obtains:

$$\left|\frac{\Delta T}{T_o}\right| = 4.5x10^{-2}|h| \tag{6.27}$$

Thus the error from using the G.I.C. approximation is about 3% , which is somewhat a larger error, and it is understandable because at 75 m/sec horizontal phase velocity is somewhat above the 45-50 m/sec upper limit that was mentioned earlier as the safe limit for using the purely G.I.C. approximation Actually in this example there is considerable interference between the G.I.C term and the wave compression term.

REFERENCES

Armstrong, E. B. , "The association of visible airglow features with a gravity wave" , J. Atmos. Terr. Phys. , 44 , 325 , (1982).

Chimonas, G. and C. O. Hines , " Atmospheric Gravity Waves launched by auroral currents" , Planet. Space Sci. , 18 , 565, (1970).

Chimonas, G. and C. O. Hines, "Doppler-ducting of atmospheric gravity waves", J. Geophys. Res., 91, 1219-1230 (1986).

Chiu, Y.T. and B.K. Ching, "The response of atmospheric and lower ionospheric layer structures to gravity waves", Geophys. Res. Lett., 5, 539-542, (1978).

Clairemidi, J. , M. Hersh and G. Moreels, "Bi-dimensional observation of waves near the mesopause at auroral latitudes", Planet. Space Sci. , 33 , 1013 , (1985).

COSPAR International Reference Atmosphere, Akadamic-Verlag, Berlin, (1972).

Crawford, J. , P. Rothwell and M. J. Taylor , " ASSESS 2: a simulated mission of Spacelab, Review article " , Nature , 275 , 17 , (1978).

Dudis, J.J. and C.A. Reber, "Composition effects in thermospheric gravity waves", Geophys. Res. Lett., 3, 727-730, (1976).

Forbes, J. M. and D. F. Gillette, "A Compendium of Theoretical Atmospheric Tidal Structures", Tech. Rept. AFGL-TR-82-01731 , (1982).

Francis, S. H., "Acoustic-gravity modes and large-scale travelling ionospheric disturbances of a realistic dissipative atmosphere", J. Geophys. Res. 78, 2278-2301, (1973a).

Francis, S. H., "Lower-atmosphere gravity modes and their relation to medium-scale travelling ionospheric disturbances", J. Geophys. Res., 78, 8289-8295, (1973b).

Francis, S. H., "A theory of medium-scale travelling ionospheric disturbances " , 79, 5245-5260 (1974).

Francis, S. H., "Global propagation of atmospheric gravity waves: A review", J. Atmos. Terr. Phys. 37, 1101-1054, (1975).

Fredrick, J. E. , "Influence of gravity wave activity on lower thermospheric photo chemistry and composition", Planet. Space Sci. , 27 , 1469 , (1979).

Fritts, D. , "Gravity wave saturation in the middle atmosphere; A review of theory and observation", Reviews of Geophysics and space physics, 22 , 275-308 (1984).

Garcia, R. R. and S. Solomon, "A numerical model of the zonally averaged dynamical and chemical structure of the middle atmosphere", J. Geophys. Res., 88, 1379-1400, (1983).

Hatfield, R., T.F. Tuan and S.M. Silverman, "On the effects of atmospheric gravity waves on profiles of H, 0_3 and OH emission", J. Geophys. Res. , 86, 2429-2437, (1981).

Hines, C.O., "Internal atmospheric gravity waves at ionospheric heights," Can. J. Phys. , 38, 1441-1481, (1960).

Holton, J. R. and W. M. Wehrbein, "A numerical model of the zonal mean circulation of the middle atmosphere", pure Appl. Geophys. , 118, 284-306, (1981).

Hunsucker, R. D. and L. H. Tveten, "Large travelling ionospheric disturbances observed a midlatitudes utilizing the high resolution h.f. backscatter technique", J. Atmos. Terr. Phys. , 29, 909 (1967).

Isler , J. , T. F. Tuan , U. Makhlouf , R. Picard and P. L. Lin,"Perturbation treatment of nonlinear airglow response to linear gravity waves II " , EOS, 69 , No. 44 , 1342 , (1988).

Lindzen, R. S. and A. Rosenthal, "On the instability of Helmholtz velocity profiles in stably stratified fluids when a lower boundary is present " , J. Geophys. Res. 81, 1561-1571, (1976).

Marion , M. J. , "Numerical Analysis , a practical approach" , Macmillan Publishing Co. , (1982) .

Midgeley, J. E. and H. B. Liemohn, "Gravity waves in a realistic atmosphere", J. Geophys. Res., 71, 3729-3748, (1966).

Moreels, G. and M. Herse , "Photographic evidence of waves around the 85 km level" , Planet. Space Sci. , 25 , 265 , (1977).

Myrabo, H. K. , C. S. Deehr and G. G. Sivjee, "large amplitute nightglow OH (8-3) band Intensity and rotational temperature variations during a 24-hour period at 78° N" , J. Geophys. Res. , 88 , 9255-9259, (1983).

Myrabo, H. K. and C. S. Deehr, "Mid-Winter Hydroxyl night airglow emission intensities in the northern polar region" , Plant. Space Sci. , 32 , 263-271 , (1984).

Peterson, A. W. and L. M. Kieffaber, "Infrared photography of OH airglow structures" , Nature , 244 , 92 , (1973).

Peterson, A. W. , "Airglow events visible to the naked eye", Appl. Optics , 18 , 3390 , (1979) Porter, H.S., S.M. Silverman and T.F. Tuan, "On the behavior of airglow under the influence of gravity waves" J. Geophys. Res. 79, 3827-3833, (1974).

Reddy, C. A., "Ducting of internal gravity waves in a temperature and wind stratified atmosphere" , Internal Gravity and Acoustic Waves - A Colloquium , NCAR Tech. Notes, TN-43, p.229-257, Natl. Center for Atmos. Res., Boulder, Colo., (1969).

Roble, R. G., R. E. Dickinson and E. C. Ridley", Seasonal and Solar cycle variations of the zonal mean circulation in the thermosphere", J. Geophys. Res., 82, 5493-5504, (1977),

Schubert, G. and R.L. Walterscheid, "A dynamical-chemical model of acoustic gravity wave induced fluctuations of hydroxyl emission", Trans. Amer. Geophys. Union, 66, 997, (1985).

Taylor, M. J. , "TV observation of mesospheric wave structure. Collection of works of the International workshop of noctilucent clouds" , Tallin, Estonian SSR, U.S.S.R. , Aug. 1984, p. 153, Tallinn "valgus", (1986).

Taylor, M. J. , M. A. Hapgood and P. Rothwell, " Observations of gravity wave propagation in the OI (557.7 nm) , Na (589.2 nm) and the near infra-red OH nightglow emissions." , Planet. Space Sci. , 35 , 413 , (1987).

Taylor, M. J. and M. A. Hapgood , "Identification of a thunderstorm as a source of short period gravity waves in the upper atmospheric nightglow emission" , Planet. Space Sci. , 36 , 975-985 , (1988).

Taylor, M. J. , "Comparison of Southampton Image data and thunderstorm maps for the Colorado Mapstar Campaign, 1988" , Mapstar report , (1989).

Tuan, T. F. and D. Tadic , "A dispersion formula for analyzing modal interference among guided and free gravity wave modes and other phenomena in a realistic atmosphere" , J. Geophys. Res. , 1648-1668 , (1982).

Wang, D. Y. and T. F. Tuan, "Brunt Doppler Ducting of small period gravity waves" , J. Geophy. Res. , 93 , 9916-9926, (1988).

Wang, D.Y. and T.F. Tuan, "Effects of dissipation and instability on guided short-period gravity waves", Trans. Amer. Geophys. Union., 67, 319, (1986).

Walterscheid, R.L., G. Schubert and J.M. Strauss, "A dynamical-chemical model of wave driven fluctuations in the OH nightglow", preprint, (1986).

Weinstock, J., "Theory of the interaction of gravity waves with $O_2(\Sigma)$ airglow", J. Geophys. Res., 83, 5175-5185, (1978).

Witt, G. , "Height structure and displacements of noctilucent clouds" , Tellus, 14 , 1-18 , (1962).

Yu, L., T.F. Tuan and H. Tai, "On 'potential' well treatment for atmospheric gravity waves", J. Geophys. Res., 85, ,1297-1305, (1980).

APPENDIXES

Appendix I

Equation (6.2) can be derived by using the usual expression for $\Delta\rho/\rho_o$, from Hines paper (1960), given by:

$$\frac{\Delta\rho}{\rho_o}=\left\{\omega^2 k_z+i\left[(\gamma-1)gk_x^2-\frac{\gamma g\omega^2}{2c^2}\right]\right\}f \qquad \text{(A1)}$$

where $f=\alpha e^{z/2H}e^{i(\omega t-k_x x-k_z z)}$

Eliminate ω by using $\omega=k_x v$ and substitute in for the scale height $H=c^2/\gamma g$ to obtain:

$$\frac{\Delta\rho}{\rho_o}=\left\{k_x^2 k_z v^2+ik_x^2c^2\left[\left(\frac{\gamma-1}{\gamma}\right)\frac{1}{H}-\frac{v^2}{2Hc^2}\right]\right\}f \qquad \text{(A2)}$$

By adding and subtracting $\left(\frac{v}{c}\right)^2\left(\frac{\gamma-1}{\gamma H}\right)$ inside the square brackets in (A2), one obtains:

$$\frac{\Delta\rho}{\rho_o}=\left\{k_x^2 k_z v^2+ik_x^2c^2\left[\left(1-\left(\frac{v}{c}\right)^2\right)\left(\frac{\gamma-1}{\gamma H}\right)-\frac{v^2}{Hc^2}\left(\frac{1}{\gamma}-\frac{1}{2}\right)\right]\right\}f \qquad \text{(A3)}$$

Introducing the vertical displacement field,

$$h = \frac{w}{i\omega} = ik_x^2 c^2 \left[1 - \left(\frac{v}{c}\right)^2\right] f \qquad \text{(A4)}$$

One get

$$\frac{\Delta\rho}{\rho_o} = \left(\frac{\gamma - 1}{\gamma}\right)\frac{h}{H} + k_x^2 v^2 \left[k_z - i\left(1 - \frac{\gamma}{2}\right)\frac{g}{c^2}\right] f \qquad \text{(A5)}$$

Finally, from Hines (1960), use $u = k_x^2 c^2 v\left[k_z - i(1 - \gamma/2)g/c^2\right]f$ to obtain:

$$\frac{\Delta\rho}{\rho_o} = \left(\frac{\gamma - 1}{\gamma}\right)\frac{h}{H} + \frac{uv}{c^2} \qquad \text{(A6)}$$

which is exactly equation (6.2).

Appendix II

Equations (6.5) and (6.6) can be obtained as follows. Use equation (A4):

$$\left|\frac{\Delta\rho_a}{\rho_o}\right| = \left(\frac{\gamma-1}{\gamma}\right)\frac{|h|}{H} = (\gamma-1)k_x^2 g\left[1-\left(\frac{\mathrm{v}}{c}\right)^2\right]|f|$$

$$= \left(\frac{\gamma-1}{\gamma}\right)\frac{1}{H}\left(\frac{c^2}{\mathrm{v}^2}-1\right)\omega^2|f| \qquad \text{(A7)}$$

Using (A1), eliminating k_x and g and substituting in $\eta = (\gamma/2 - 1)\, g/c^2$, to obtain:

$$\left|\frac{\Delta\rho}{\rho_o}\right| = \left\{k_z^2 + \left[\left(\frac{\gamma-1}{\gamma}\right)\frac{1}{H}\left(\frac{c^2}{\mathrm{v}^2}-1\right)+\eta\right]^2\right\}^{1/2}\omega^2|f| \qquad \text{(A8)}$$

Using the dispersion relation (Hines, 1960), and letting $\varepsilon = (c^2/\mathrm{v}^2) - 1$, so one have:

$$k_z^2 = \frac{\omega_b^2-\omega^2}{\mathrm{v}^2} - \frac{\omega_a^2-\omega^2}{c^2} = \frac{\omega_b^2-\omega^2}{c^2}\varepsilon - \eta^2 \qquad \text{(A9)}$$

where $\eta^2 = \dfrac{\omega_a^2-\omega_b^2}{c^2}$

Thus,

$$\left|\frac{\Delta\rho_a}{\Delta\rho}\right| = \frac{\left(\frac{\gamma-1}{\gamma}\right)\frac{\varepsilon}{H}}{\left\{\frac{\omega_b^2-\omega^2}{c^2}\varepsilon + \left[\left(\frac{\gamma-1}{\gamma}\right)\frac{1}{H}\right]^2\varepsilon^2 + \frac{(\gamma-1)\eta}{\gamma H}\varepsilon^2\right\}^{1/2}}$$

or

$$\left|\frac{\Delta\rho_a}{\Delta\rho}\right| = \left\{\frac{\left(\frac{\gamma-1}{\gamma}\right)^2 \frac{\varepsilon}{H^2}}{\frac{\omega_b^2-\omega^2}{c^2} + \left[\left(\frac{\gamma-1}{\gamma}\right)\frac{1}{H}\right]^2 \varepsilon - \left(\frac{\gamma-1}{\gamma}\right)\frac{(2-\gamma)g}{Hc^2}}\right\}^{1/2} \qquad \text{(A10)}$$

Using $\omega_b^2 = (\gamma-1)g^2/c^2$ and divide it from the numerator and denominator, one obtains:

$$\left|\frac{\Delta\rho_a}{\Delta\rho}\right| = \left\{\frac{(\gamma-1)\left(1-\left(\frac{\mathrm{v}}{c}\right)^2\right)}{(\gamma-1)-\left(\frac{\omega}{\omega_b}\right)^2\left(\frac{\mathrm{v}}{c}\right)^2}\right\}^{1/2} \qquad \text{(A11)}$$

which is exactly equation (6.5)

To compute $|\Delta\rho_c| / |\Delta\rho|$, note that:

$$\frac{\Delta\rho_c}{\rho_o} = \frac{u\mathrm{v}}{c^2} = \frac{\mathrm{v}}{c^2}\left\{\omega k_x c^2\left[k_z - i\left(1-\frac{\gamma}{2}\right)\frac{g}{c^2}\right]\right\}f \qquad \text{(A12)}$$

Where again , the polarization relation for u from Hines (1960) was used. Substituting for η one gets:

$$\frac{\Delta\rho_c}{\rho_o} = \frac{\mathrm{v}}{c^2}\left\{\omega k_x c^2\left[k_z + i\eta\right]\right\}f \qquad \text{(A13)}$$

Using (A8) and (A13), one gets:

$$\left|\frac{\Delta\rho_c}{\Delta\rho}\right| = \left\{\frac{k_z^2+\eta^2}{k_z^2+\left[\frac{(\gamma-1)}{\gamma}\frac{1}{H}\varepsilon+\eta\right]^2}\right\}^{1/2} \tag{A14}$$

Using (A9) we obtain:

$$\left|\frac{\Delta\rho_c}{\Delta\rho}\right| = \left\{\frac{\frac{\omega_b^2-\omega^2}{c^2}\varepsilon}{\frac{\omega_b^2-\omega^2}{c^2}\varepsilon-\eta^2+\left(\frac{\gamma-1}{\gamma}\frac{\varepsilon}{H}+\eta\right)^2}\right\}^{1/2}$$

so

$$\left|\frac{\Delta\rho_c}{\Delta\rho}\right| = \left\{\frac{1-\left(\omega/\omega_b\right)^2}{(\gamma-1)-\left(\omega/\omega_b\right)^2\left(\mathrm{v}/\mathrm{c}\right)^2}\right\}^{1/2}\left(\frac{\mathrm{v}}{c}\right) \tag{A15}$$

which is equation (6.6)

Appendix III

Using equations (6.12), (A4) and Hines polarization relation for u (Hines 1960), one can obtain:

$$\frac{\Delta T}{T_o}=(\gamma-1)\left\{\frac{\mathrm{v}}{\mathrm{c}^2}\left[\omega k_x c^2\left(k_z+i\eta\right)\right]-ik_x^2 g\left(\frac{\mathrm{v}}{\mathrm{c}}\right)^2\left(\frac{c^2}{\mathrm{v}^2}-1\right)\right\}f \qquad \text{(A16)}$$

Since $\frac{\Delta T_a}{T_o}=-\frac{\Delta\rho_a}{\rho_0}$, one can use equations (A7) and (A16) to obtain:

$$\left|\frac{\Delta T_a}{\Delta T}\right|=\frac{(\gamma-1)\left(k_x^2\mathrm{v}^2 g/c^2\right)\varepsilon}{(\gamma-1)k_x^2\mathrm{v}^2\left[k_z^2+\left(\eta-\left(g/c^2\right)\varepsilon\right)^2\right]^{1/2}} \qquad \text{(A17)}$$

Using again the dispersion relation for k_z, equation (A9) , to obtain:

$$\left|\frac{\Delta T_a}{\Delta T}\right|=\left\{\frac{1-\left(\mathrm{v}/\mathrm{c}\right)^2}{1-(\gamma-1)\left(\omega/\omega_b\right)^2\left(\mathrm{v}/\mathrm{c}\right)^2}\right\}^{1/2} \qquad \text{(A18)}$$

Equation (6.16) can be similarly obtained. The denominator is the same as (A18) as expected , but the numerator is given by $|(\gamma-1)uv/c^2|$ which is identical to (A15) except for the additional $(\gamma-1)$ factor.

Appendix IV

The K. E. Density is given by:

$$K.E. = \frac{1}{4}\rho_o\left(|u|^2 + |w|^2\right) \qquad \text{(A19)}$$

From Hines polarization relations (Hines, 1960), and the definition of η , one can write:

$$u = \omega k_x c^2 [k_z + i\eta] f \qquad \text{(A20)}$$

$$w = -\omega k_x^2 c^2 \left[1 - \left(\mathrm{v}/\mathrm{c}\right)^2\right] f \qquad \text{(A21)}$$

so

$$|u|^2 = \frac{k_z^2 + \eta^2}{k_x^2\left[1 - \left(\mathrm{v}/\mathrm{c}\right)^2\right]^2}|w|^2 \qquad \text{(A22)}$$

From the dispersion relation

$$\left(\frac{k_z}{k_x}\right)^2 = \frac{\omega_b^2 - \omega^2}{\omega^2} - \left(\frac{\mathrm{v}}{\mathrm{c}}\right)^2 \frac{\omega_a^2 - \omega^2}{\omega^2} \qquad \text{(A23)}$$

$$\left(\frac{\eta}{k_x}\right)^2 = \left(\frac{\mathrm{v}}{\mathrm{c}}\right)^2 \frac{\omega_a^2 - \omega_b^2}{\omega^2} \qquad \text{(A24)}$$

Hence,

$$|u|^2 + |w|^2 = |w|^2 \left\{ 1 + \frac{\left[\left(\omega_b^2 \big/ \omega^2 \right) - 1 \right]}{\left[1 - \left(\mathrm{v} \big/ \mathrm{c} \right)^2 \right]} \right\} \qquad \text{(A25)}$$

The total K.E. then becomes:

$$K.E. = \frac{1}{4} \rho_o \omega_b^2 |h|^2 \left\{ \frac{\left[1 - \left(\omega \big/ \omega_b \right)^2 \left(\mathrm{v} \big/ \mathrm{c} \right)^2 \right]}{\left[1 - \left(\mathrm{v} \big/ \mathrm{c} \right)^2 \right]} \right\} \qquad \text{(A26)}$$

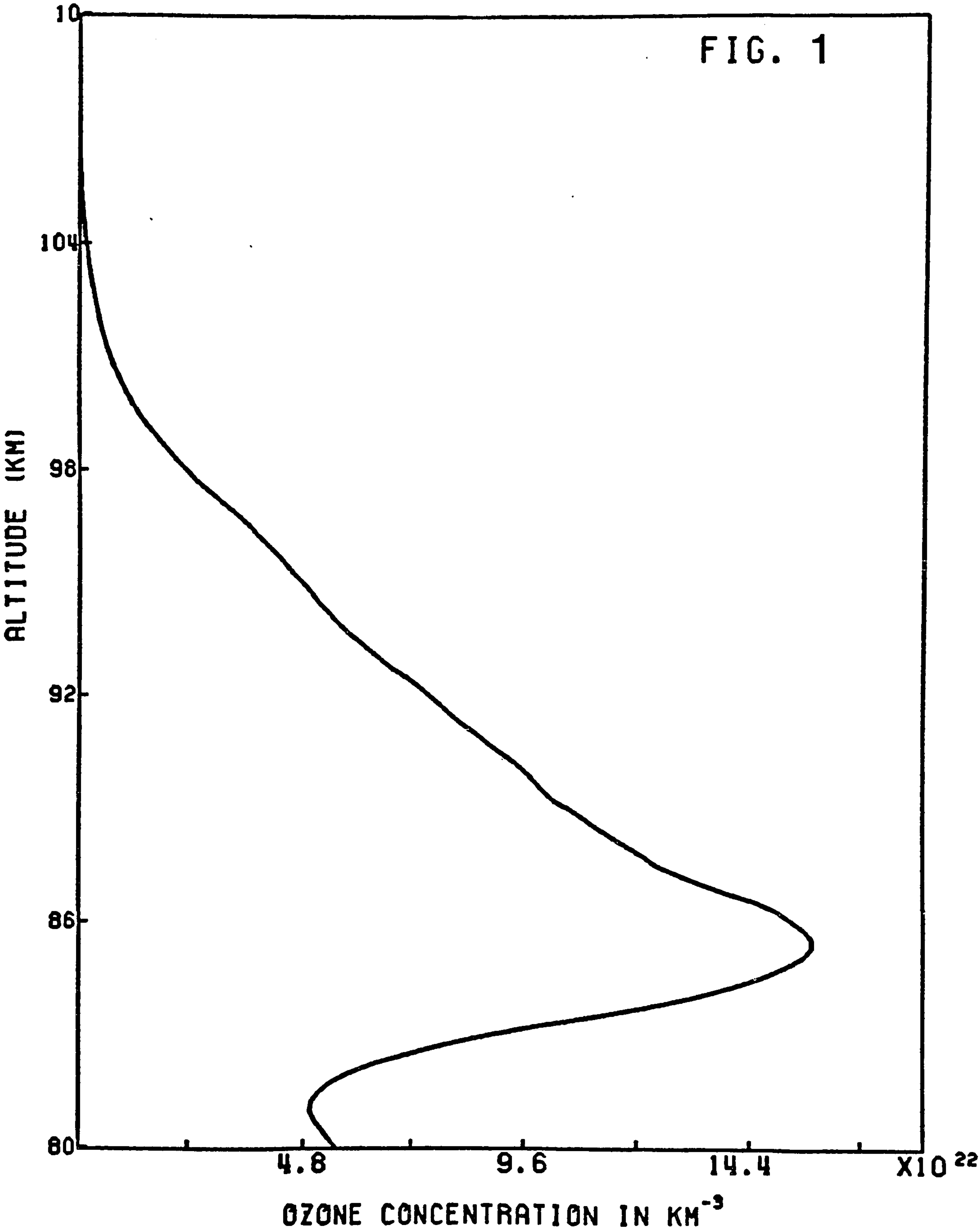
10
104
98
92
86
80
ALTITUDE (KM)
4.8
9.6
14.4
X10 22
OZONE CONCENTRATION IN KM-3

FIG. 1

Fig. 1.1

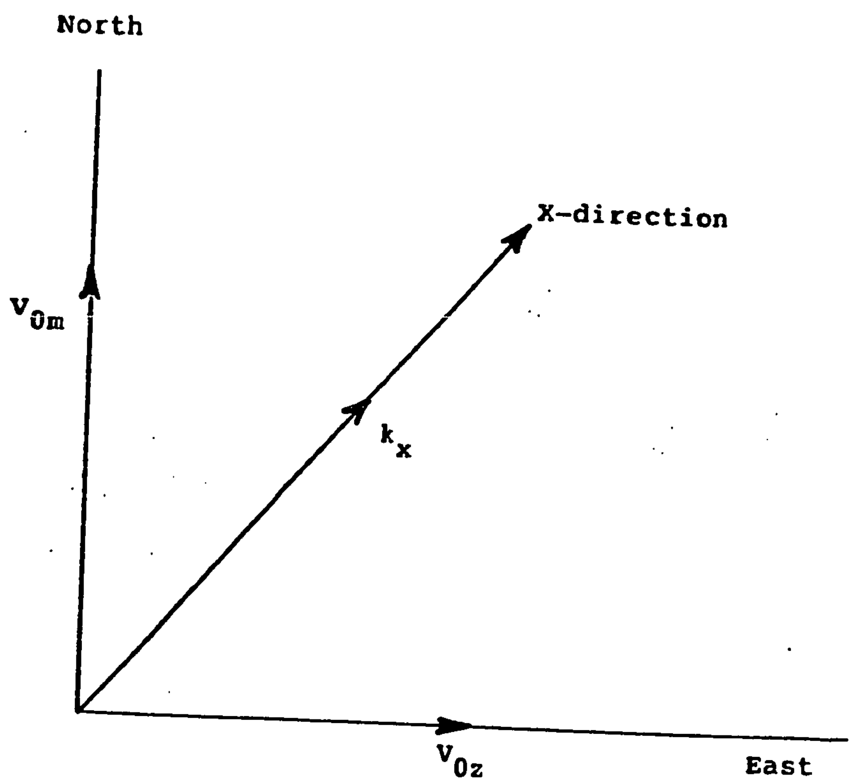

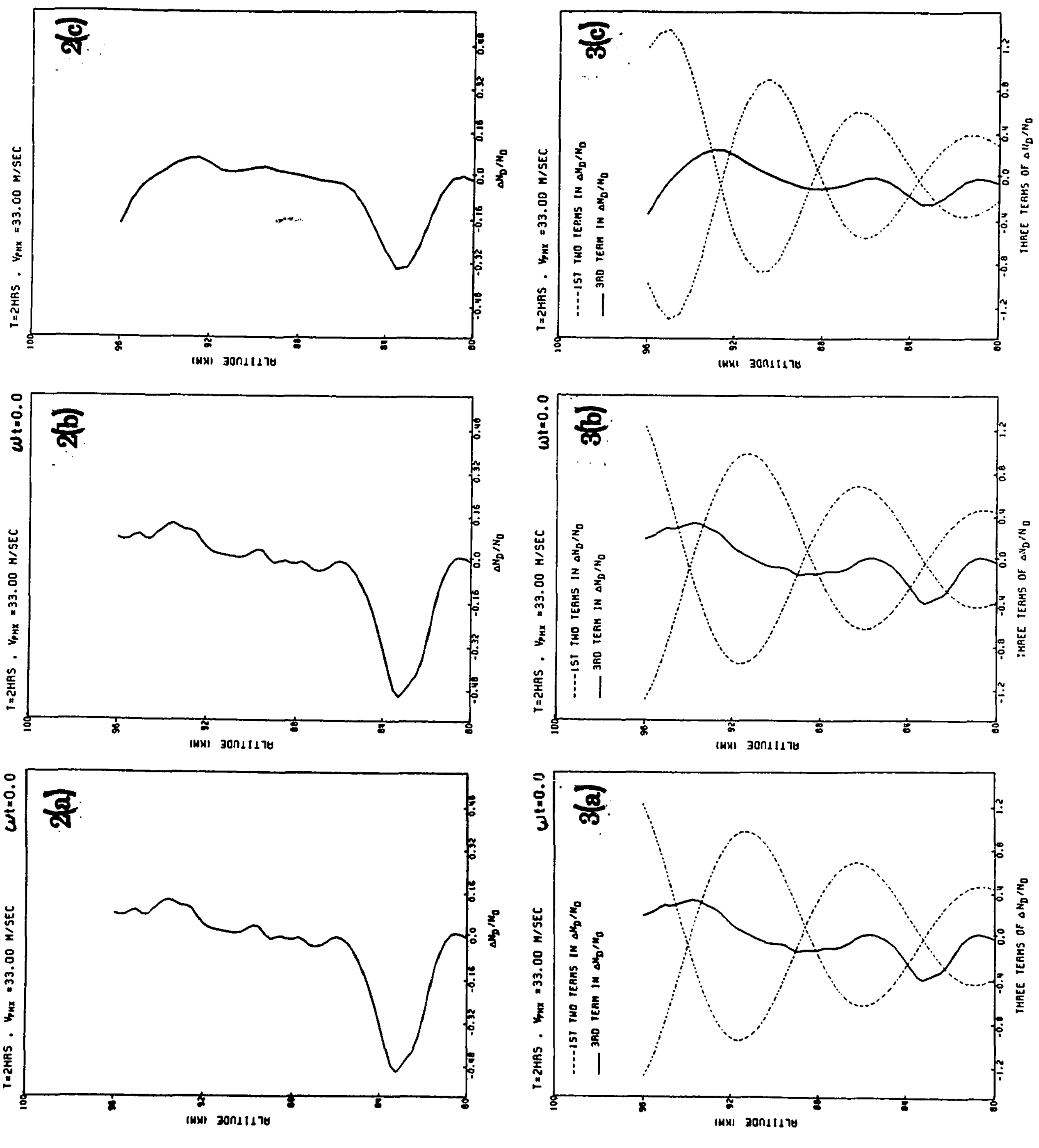

T=2HRS . VPMX =33.00 M/SEC
ωt=0.0
2(a)
2(b)
2(c)
3(a)
3(b)
3(c)
ALTITUDE (KM)
ΔND/ND
----1ST TWO TERMS IN ΔND/ND
—— 3RD TERM IN ΔND/ND
THREE TERMS OF ΔND/ND

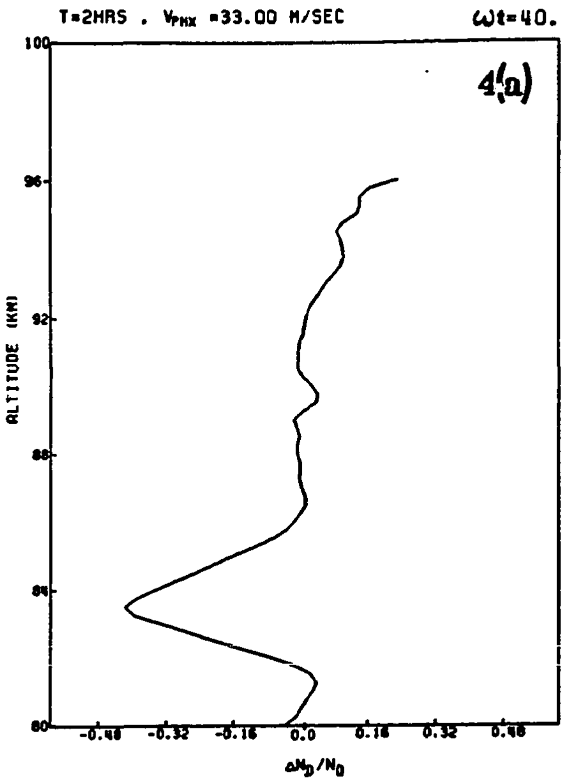
T=2HRS . V_{PHX} =33.00 M/SEC
ωt=40.
4(a)
ALTITUDE (KM)
$\Delta N_D/N_0$

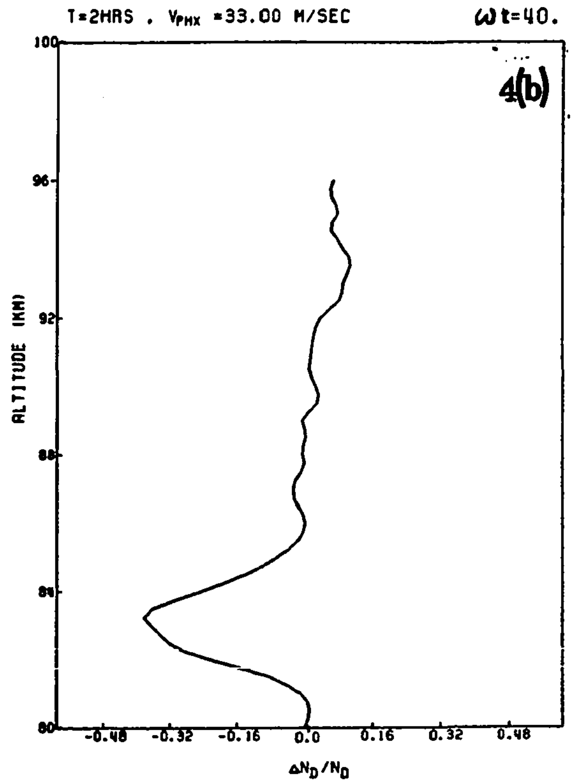
T=2HRS . V_{PHX} =33.00 M/SEC
ωt=40.
4(b)
ALTITUDE (KM)
$\Delta N_D/N_0$

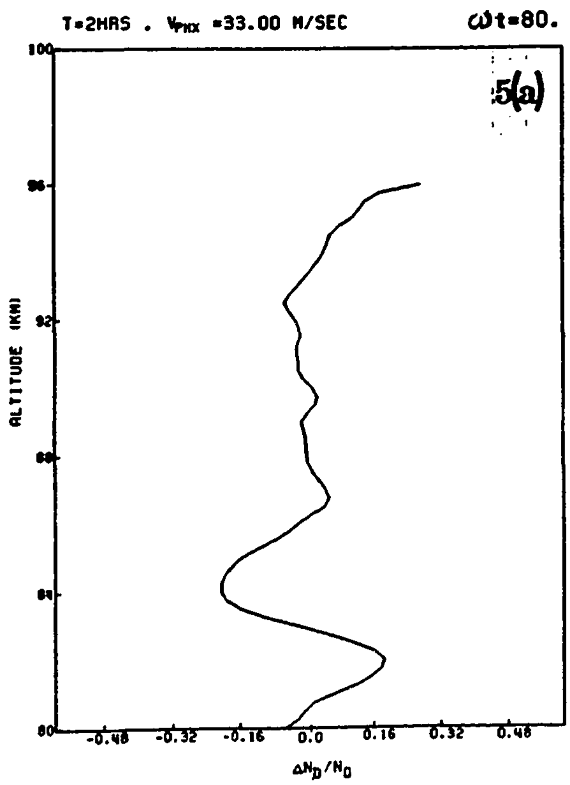
T=2HRS . V_{PHX} =33.00 M/SEC
ωt=80.
5(a)
ALTITUDE (KM)
$\Delta N_D/N_0$

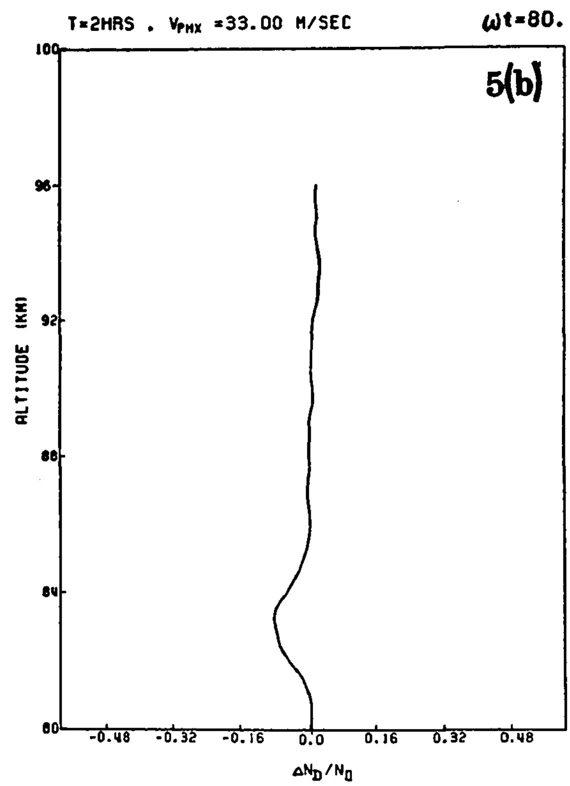
T=2HRS . V_{PHX} =33.00 M/SEC
ωt=80.
5(b)
ALTITUDE (KM)
$\Delta N_D/N_0$

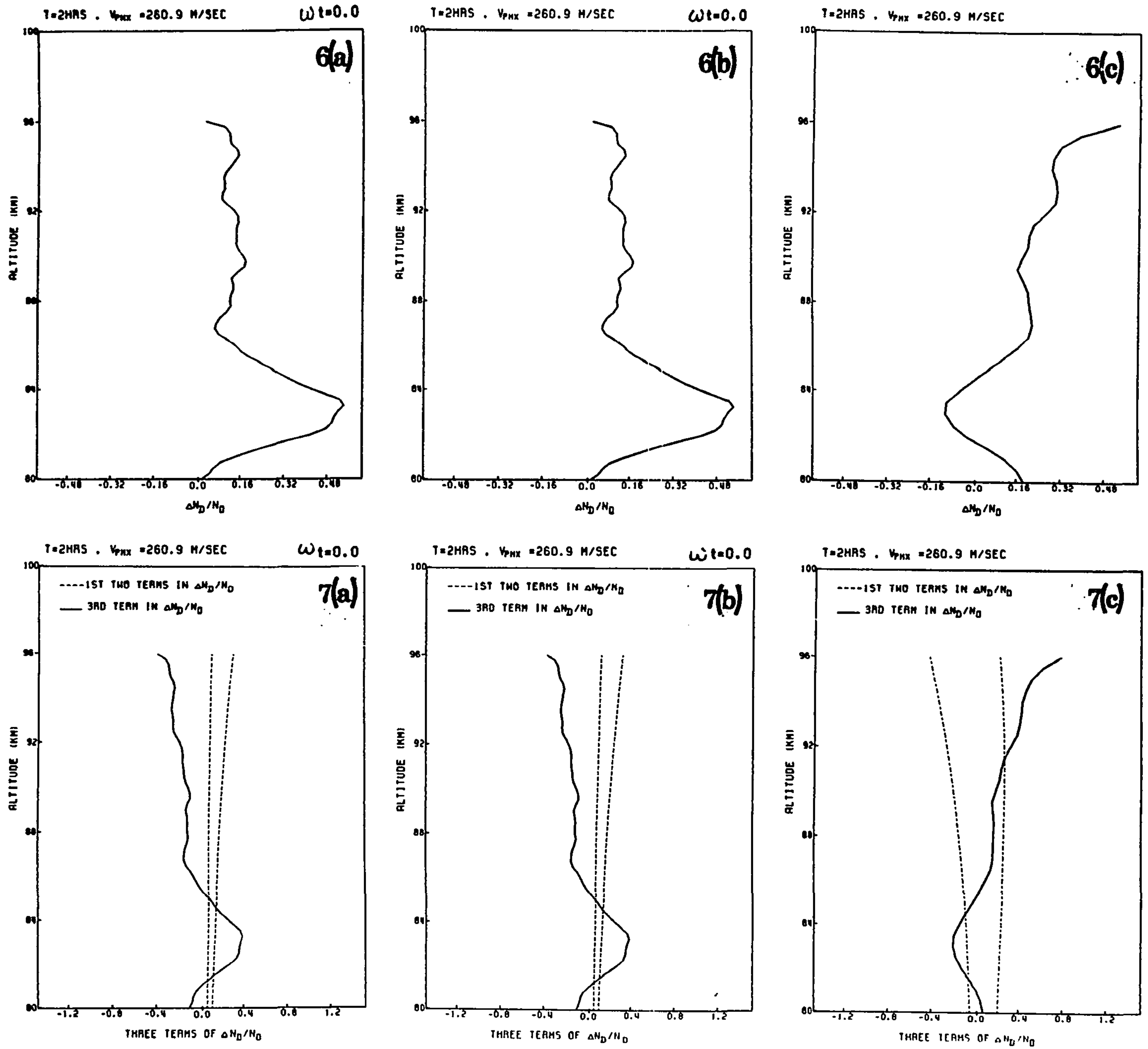
T=2HRS . V_{PMX} =260.9 M/SEC
ωt=0.0
6(a)
6(b)
6(c)
ALTITUDE (KM)
$\Delta N_D/N_0$
7(a)
7(b)
7(c)
----1ST TWO TERMS IN $\Delta N_D/N_0$
3RD TERM IN $\Delta N_D/N_0$
THREE TERMS OF $\Delta N_D/N_0$

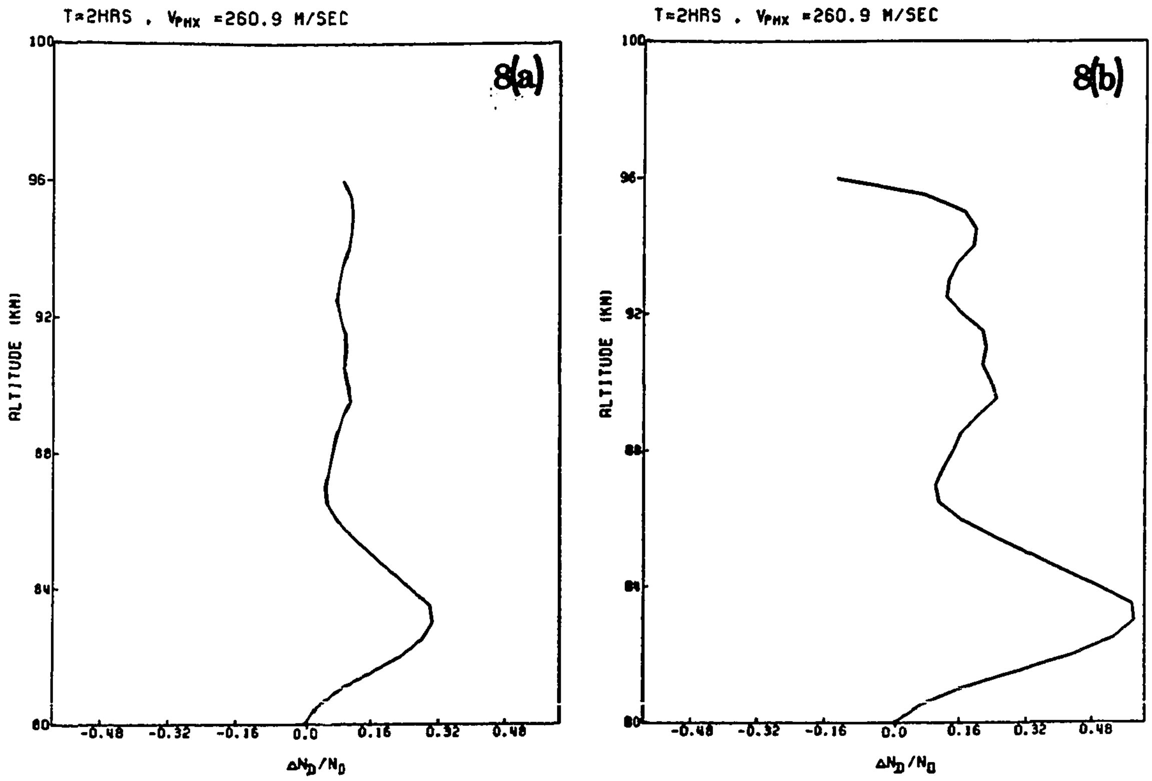
T=2HRS , V_{PMX} =260.9 M/SEC
8(a)
ALTITUDE (KM)
100
96
92
88
84
80
-0.48 -0.32 -0.16 0.0 0.16 0.32 0.48
$\Delta N_D/N_D$
T=2HRS , V_{PMX} =260.9 M/SEC
8(b)
ALTITUDE (KM)
100
96
92
88
84
80
-0.48 -0.32 -0.16 0.0 0.16 0.32 0.48
$\Delta N_D/N_D$

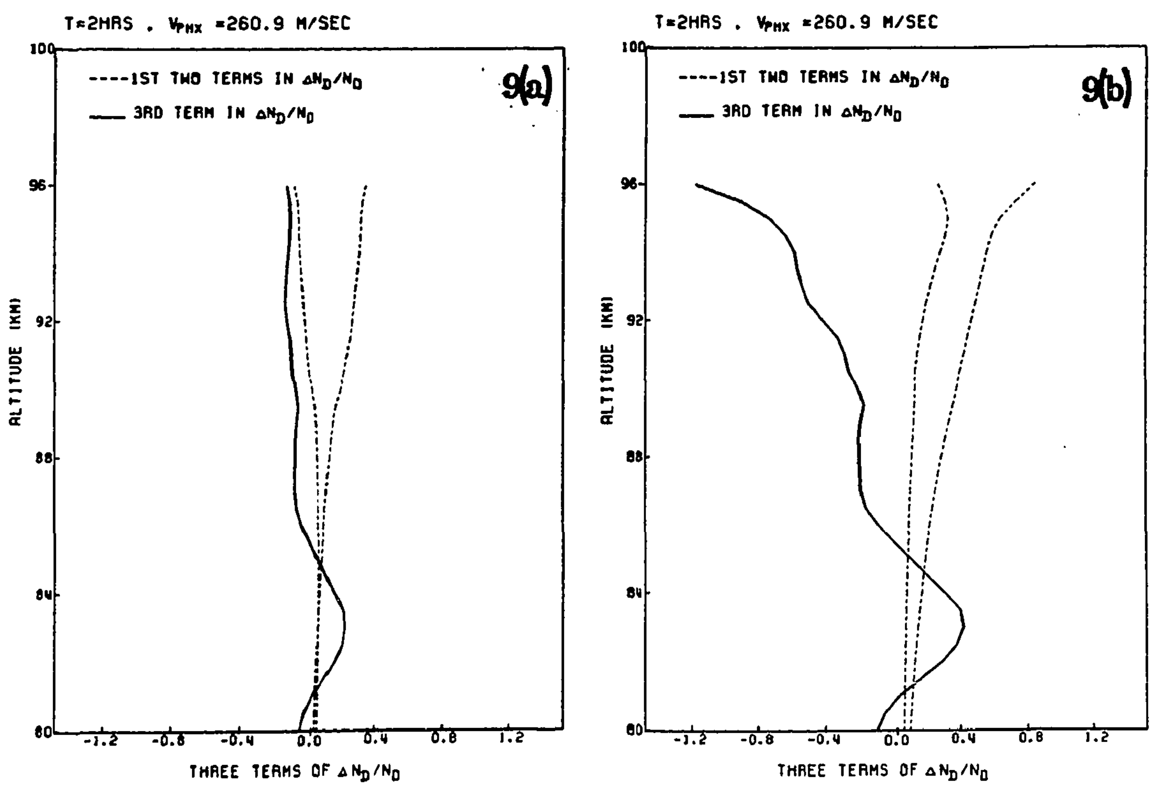
T=2HRS , V_{PMX} =260.9 M/SEC
9(a)
----1ST TWO TERMS IN $\Delta N_D/N_D$
3RD TERM IN $\Delta N_D/N_D$
ALTITUDE (KM)
100
96
92
88
84
80
-1.2 -0.8 -0.4 0.0 0.4 0.8 1.2
THREE TERMS OF $\Delta N_D/N_D$
T=2HRS , V_{PMX} =260.9 M/SEC
9(b)
----1ST TWO TERMS IN $\Delta N_D/N_D$
3RD TERM IN $\Delta N_D/N_D$
ALTITUDE (KM)
100
96
92
88
84
80
-1.2 -0.8 -0.4 0.0 0.4 0.8 1.2
THREE TERMS OF $\Delta N_D/N_D$

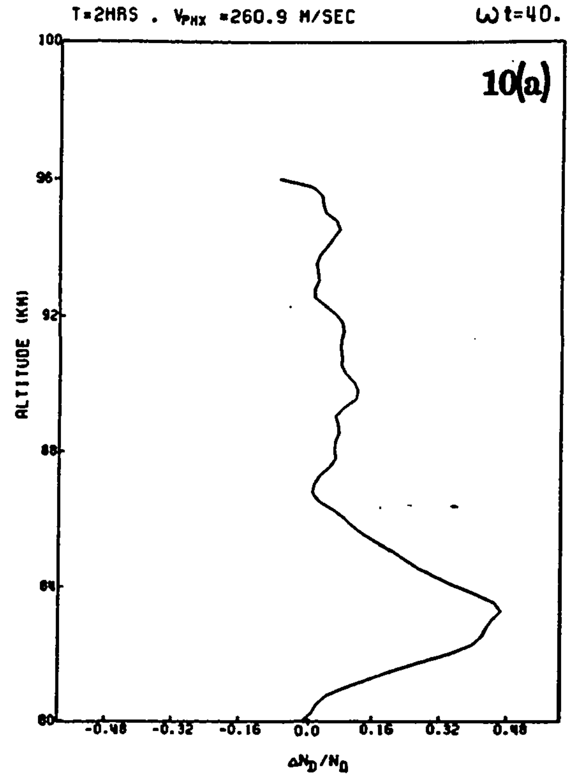
T=2HRS . V_PHX =260.9 M/SEC
ωt=40.
10(a)
ALTITUDE (KM)
100
96
92
88
84
80
-0.48 -0.32 -0.16 0.0 0.16 0.32 0.48
ΔN_D/N_0

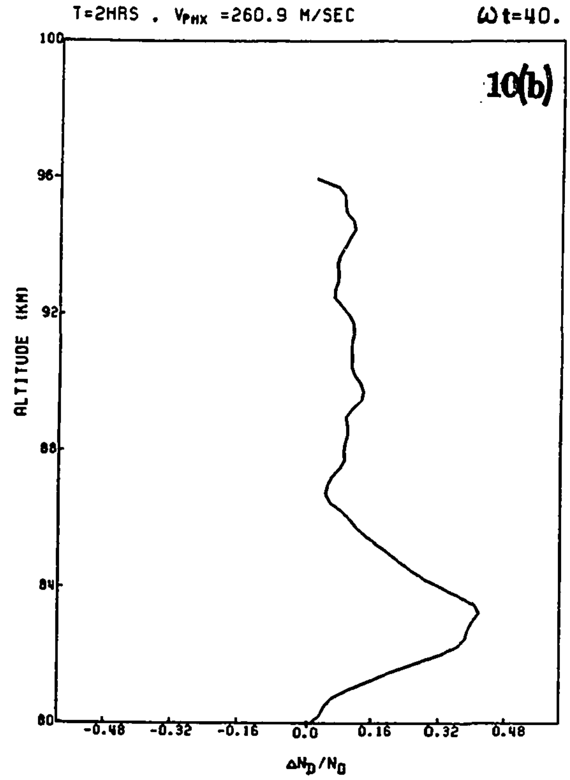
T=2HRS . V_PHX =260.9 M/SEC
ωt=40.
10(b)
ALTITUDE (KM)
100
96
92
88
84
80
-0.48 -0.32 -0.16 0.0 0.16 0.32 0.48
ΔN_D/N_0

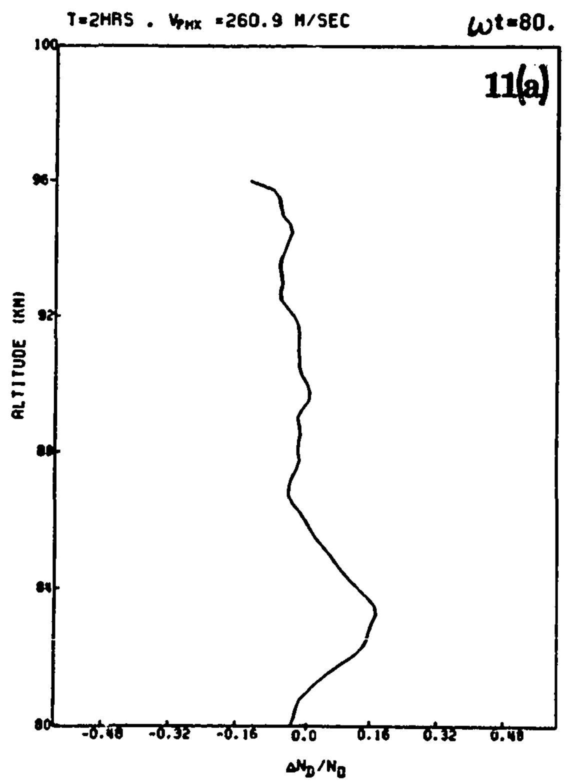
T=2HRS . V_PHX =260.9 M/SEC
ωt=80.
11(a)
ALTITUDE (KM)
100
96
92
88
84
80
-0.48 -0.32 -0.16 0.0 0.16 0.32 0.48
ΔN_D/N_0

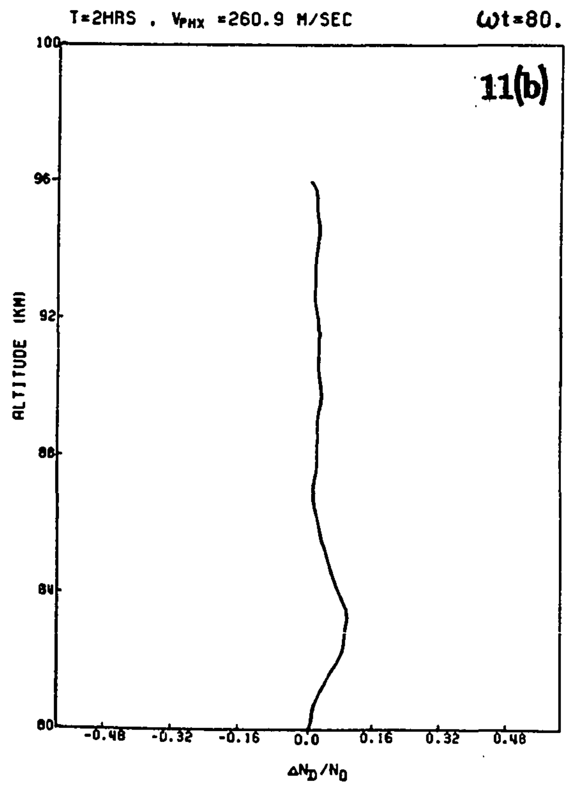
T=2HRS . V_PHX =260.9 M/SEC
ωt=80.
11(b)
ALTITUDE (KM)
100
96
92
88
84
80
-0.48 -0.32 -0.16 0.0 0.16 0.32 0.48
ΔN_D/N_0

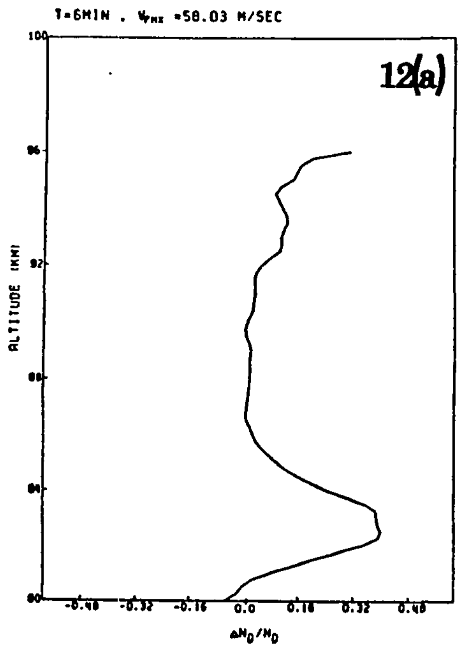
T=6MIN . V_{PMX} =58.03 M/SEC
12(a)
ALTITUDE (KM)
$\Delta N_D/N_D$

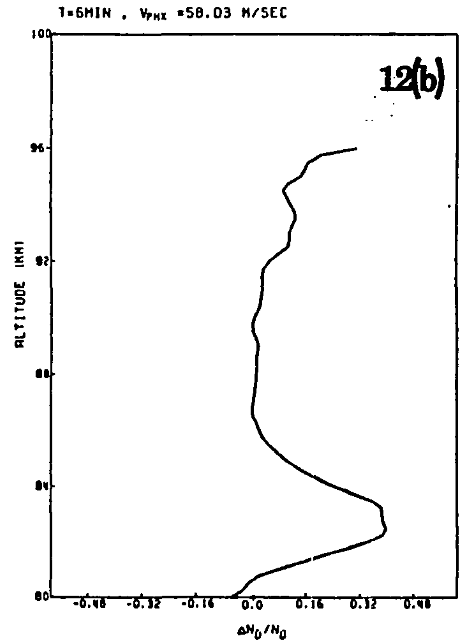
T=6MIN . V_{PMX} =58.03 M/SEC
12(b)
ALTITUDE (KM)
$\Delta N_D/N_D$

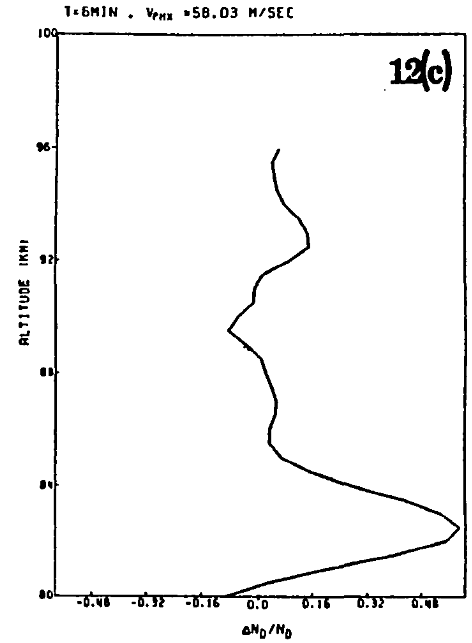
T=6MIN . V_{PMX} =58.03 M/SEC
12(c)
ALTITUDE (KM)
$\Delta N_D/N_D$

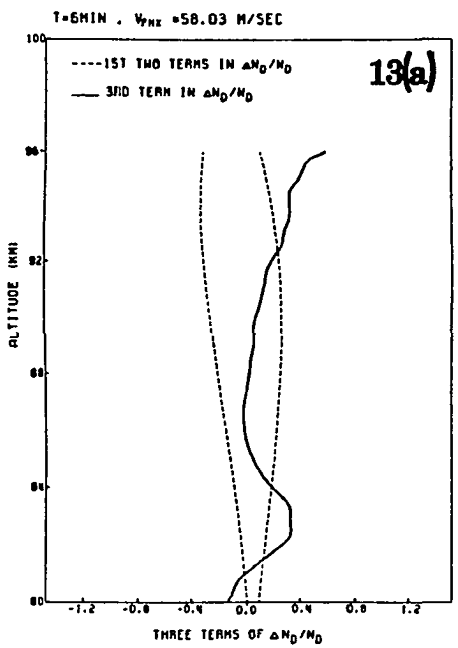
T=6MIN . V_{PMX} =58.03 M/SEC
----1ST TWO TERMS IN $\Delta N_D/N_D$
—— 3RD TERM IN $\Delta N_D/N_D$
13(a)
ALTITUDE (KM)
THREE TERMS OF $\Delta N_D/N_D$

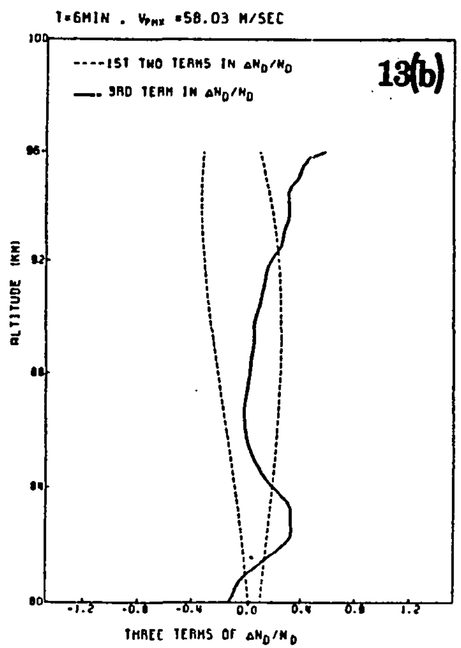
T=6MIN . V_{PMX} =58.03 M/SEC
----1ST TWO TERMS IN $\Delta N_D/N_D$
—— 3RD TERM IN $\Delta N_D/N_D$
13(b)
ALTITUDE (KM)
THREE TERMS OF $\Delta N_D/N_D$

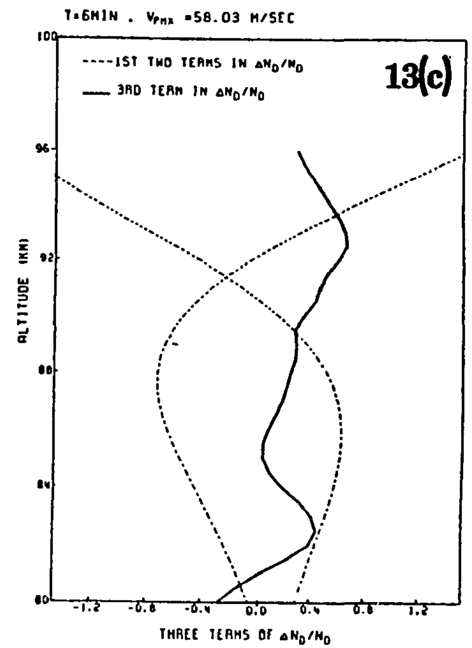
T=6MIN . V_{PMX} =58.03 M/SEC
----1ST TWO TERMS IN $\Delta N_D/N_D$
—— 3RD TERM IN $\Delta N_D/N_D$
13(c)
ALTITUDE (KM)
THREE TERMS OF $\Delta N_D/N_D$

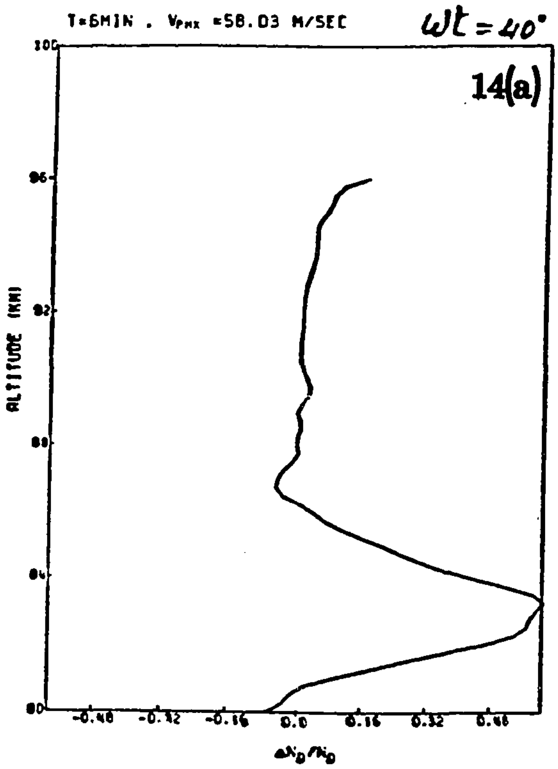
T=6MIN . VPMX =58.03 M/SEC
ωt = 40°
14(a)
ALTITUDE (KM)
100
96
92
88
84
80
-0.48
-0.32
-0.16
0.0
0.16
0.32
0.48
ΔND/ND

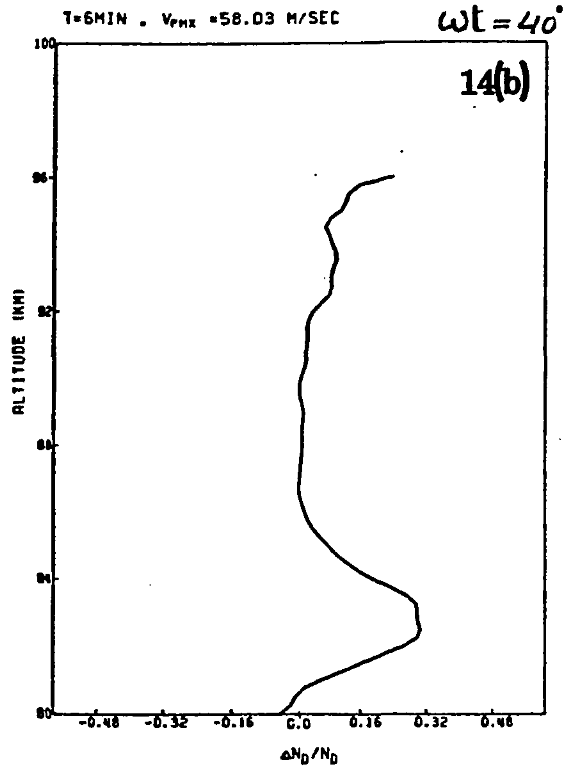
T=6MIN . VPMX =58.03 M/SEC
ωt = 40°
14(b)
ALTITUDE (KM)
100
96
92
88
84
80
-0.48
-0.32
-0.16
0.0
0.16
0.32
0.48
ΔND/ND

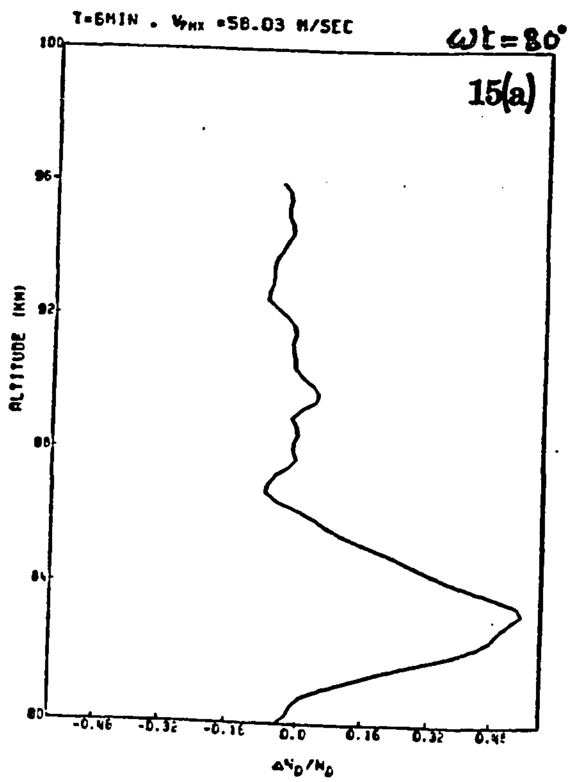
T=6MIN . VPMX =58.03 M/SEC
ωt = 80°
15(a)
ALTITUDE (KM)
100
96
92
88
84
80
-0.48
-0.32
-0.16
0.0
0.16
0.32
0.48
ΔND/ND

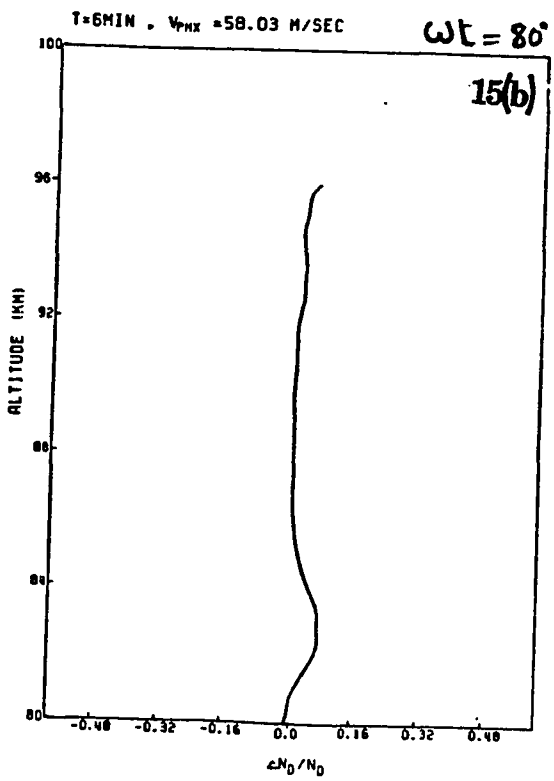
T=6MIN . VPMX =58.03 M/SEC
ωt = 80°
15(b)
ALTITUDE (KM)
100
96
92
88
84
80
-0.48
-0.32
-0.16
0.0
0.16
0.32
0.48
ΔND/ND

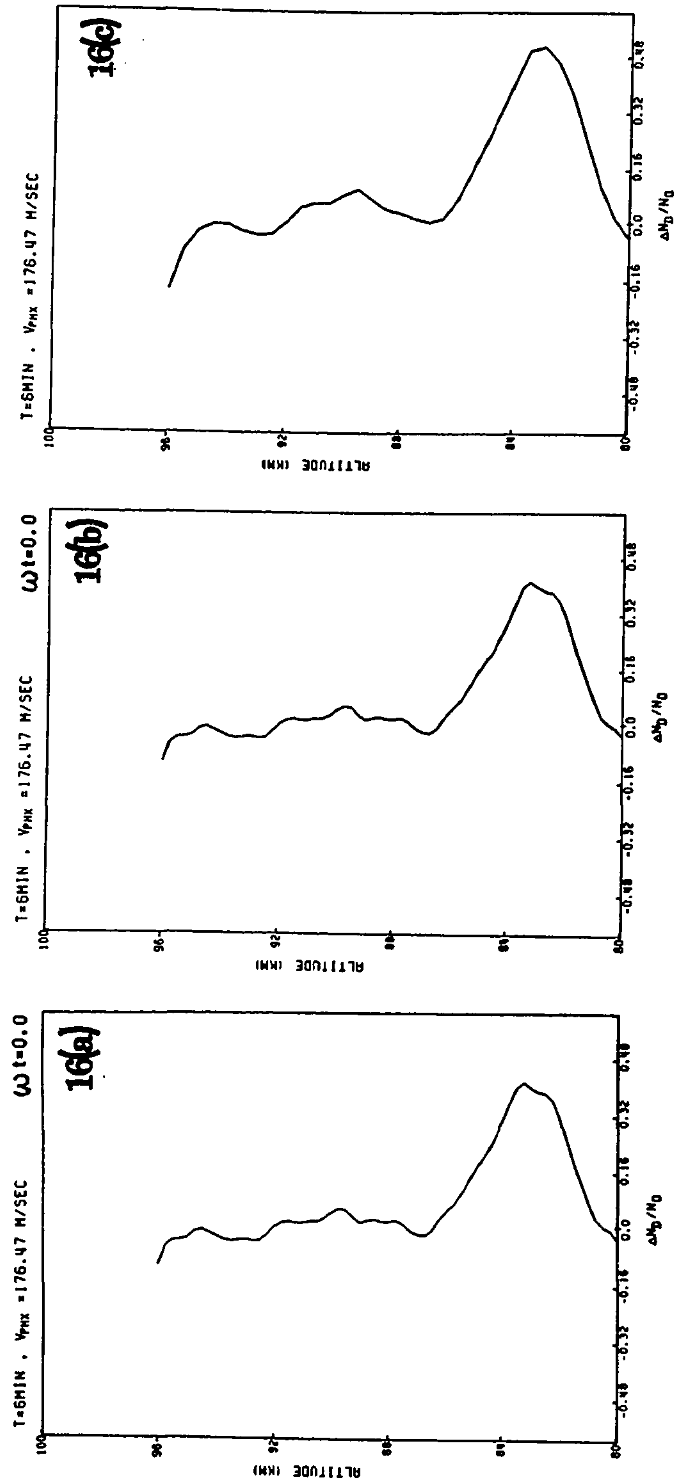

16(a)
16(b)
16(c)
T=6MIN . V_PMX =176.47 M/SEC
ωt=0.0
ALTITUDE (KM)
ΔN_D/N_0

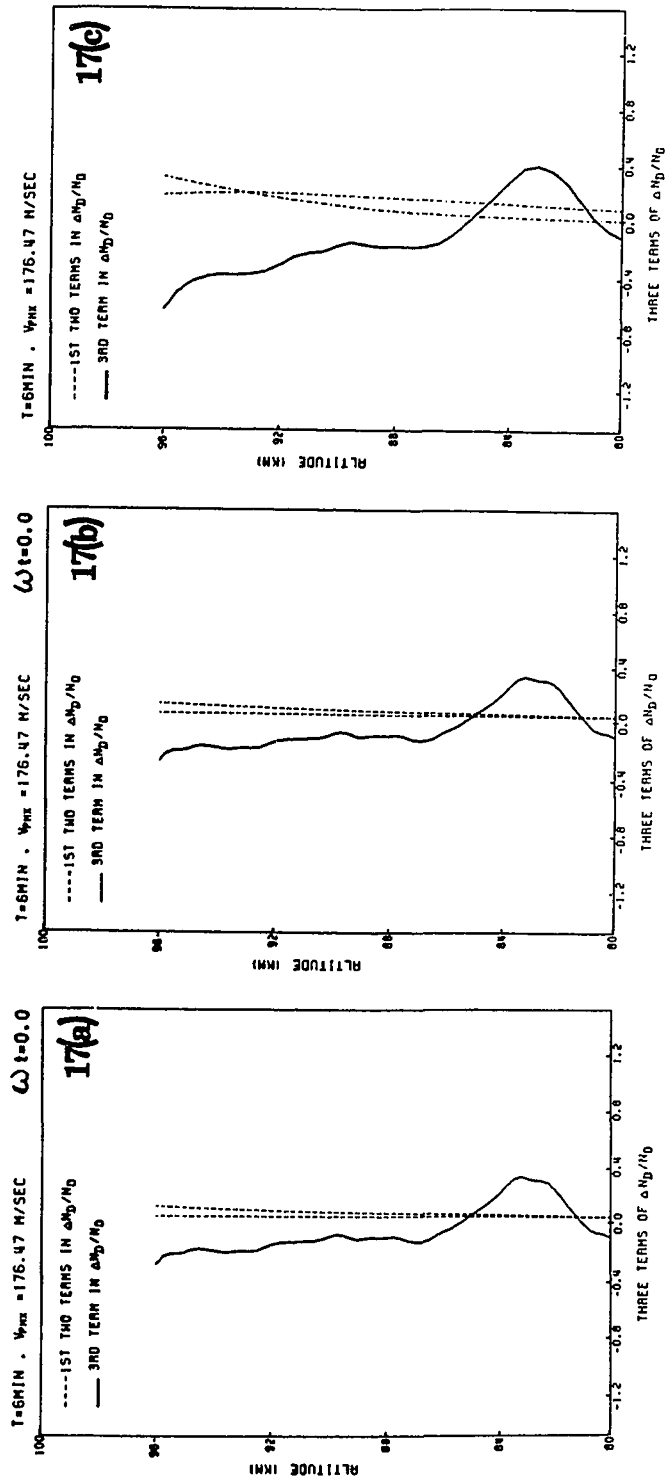

17(a)
17(b)
17(c)
T=6MIN . V_PMX =176.47 M/SEC
ωt=0.0
----1ST TWO TERMS IN ΔN_D/N_0
—— 3RD TERM IN ΔN_D/N_0
ALTITUDE (KM)
THREE TERMS OF ΔN_D/N_0

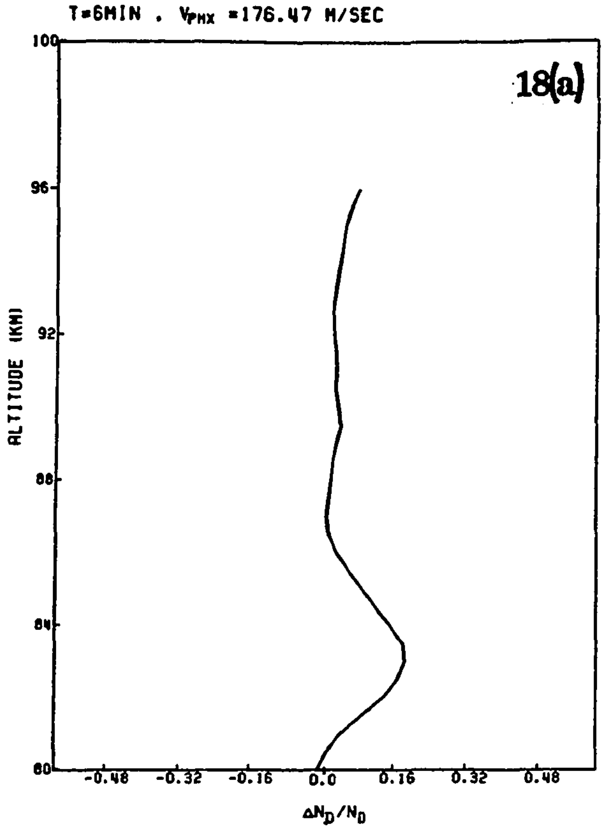
T=6MIN . V_{PMX} =176.47 M/SEC
18(a)
ALTITUDE (KM)
100
96
92
88
84
80
-0.48
-0.32
-0.16
0.0
0.16
0.32
0.48
$\Delta N_D/N_D$

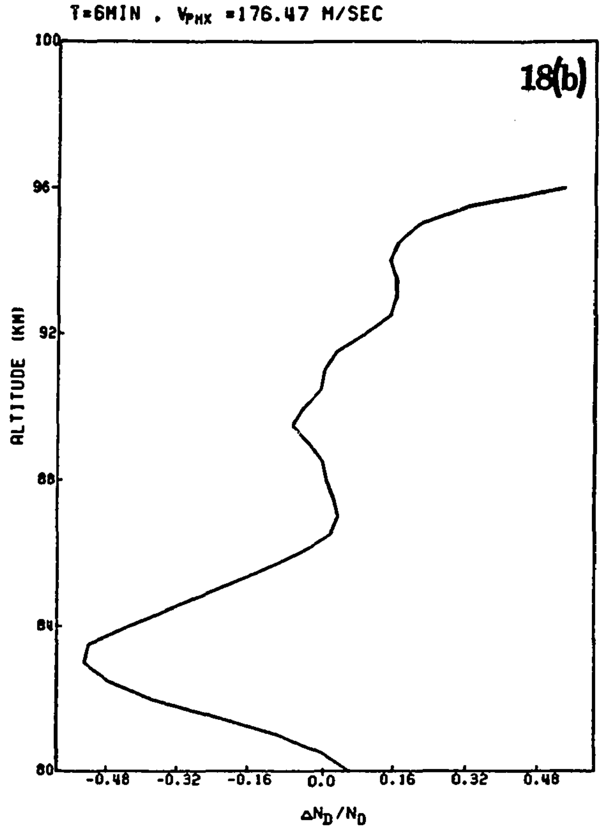
T=6MIN . V_{PMX} =176.47 M/SEC
18(b)
ALTITUDE (KM)
100
96
92
88
84
80
-0.48
-0.32
-0.16
0.0
0.16
0.32
0.48
$\Delta N_D/N_D$

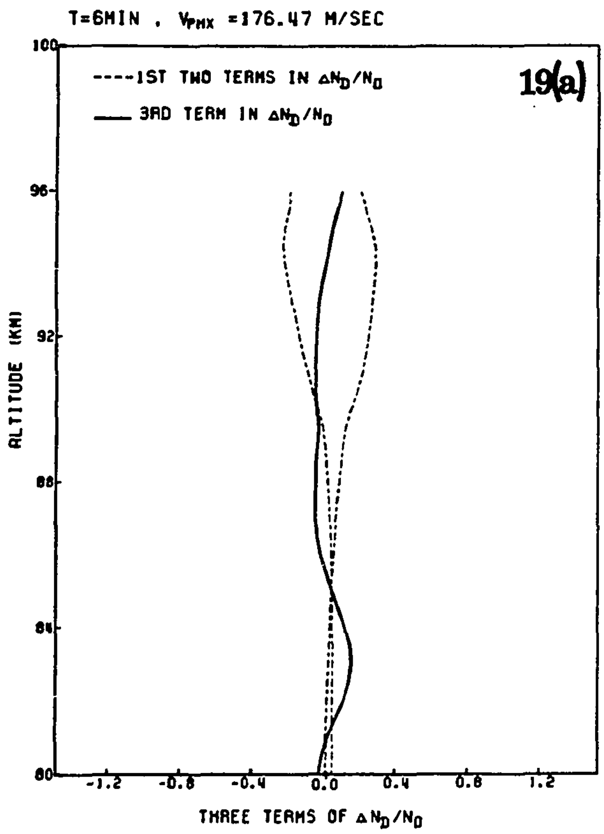
T=6MIN . V_{PMX} =176.47 M/SEC
----1ST TWO TERMS IN $\Delta N_D/N_D$
—— 3RD TERM IN $\Delta N_D/N_D$
19(a)
ALTITUDE (KM)
100
96
92
88
84
80
-1.2
-0.8
-0.4
0.0
0.4
0.8
1.2
THREE TERMS OF $\Delta N_D/N_D$

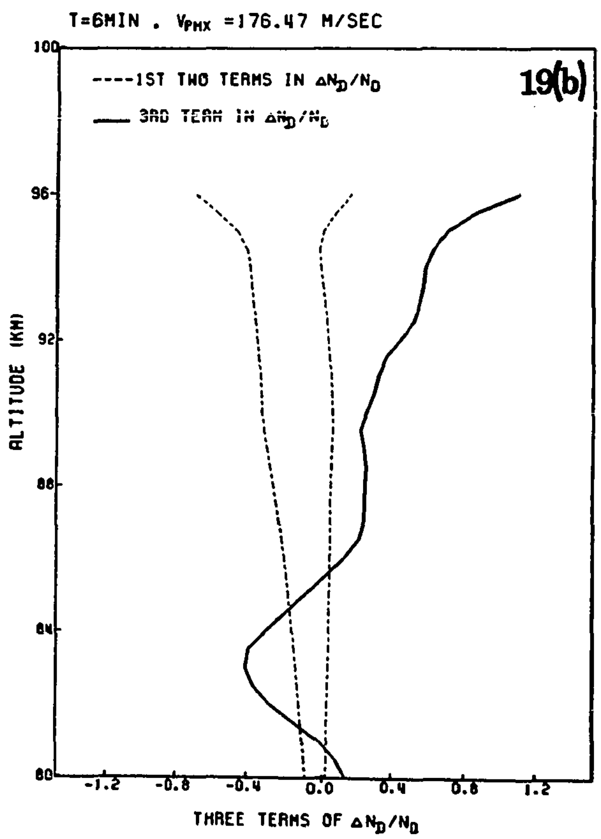
T=6MIN . V_{PMX} =176.47 M/SEC
----1ST TWO TERMS IN $\Delta N_D/N_D$
—— 3RD TERM IN $\Delta N_D/N_D$
19(b)
ALTITUDE (KM)
100
96
92
88
84
80
-1.2
-0.8
-0.4
0.0
0.4
0.8
1.2
THREE TERMS OF $\Delta N_D/N_D$

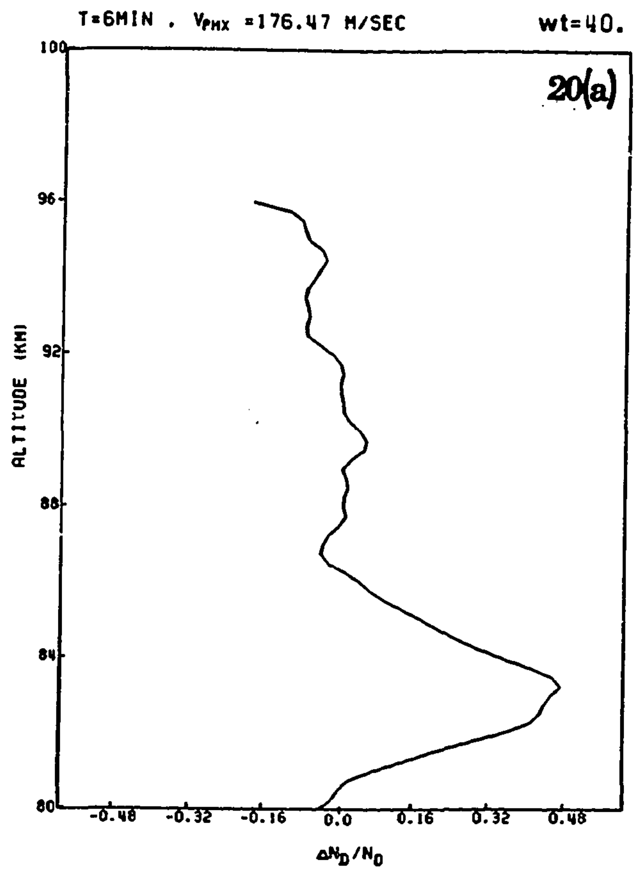
T=6MIN . V_PMX =176.47 M/SEC
wt=40.
20(a)
ALTITUDE (KM)
100
96
92
88
84
80
-0.48
-0.32
-0.16
0.0
0.16
0.32
0.48
ΔN_D/N_D

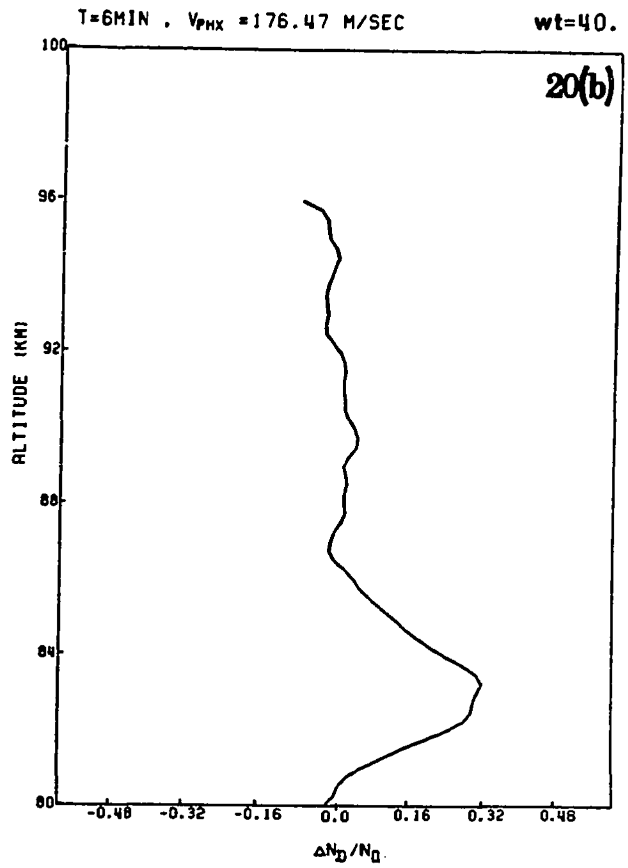
T=6MIN . V_PMX =176.47 M/SEC
wt=40.
20(b)
ALTITUDE (KM)
100
96
92
88
84
80
-0.48
-0.32
-0.16
0.0
0.16
0.32
0.48
ΔN_D/N_D

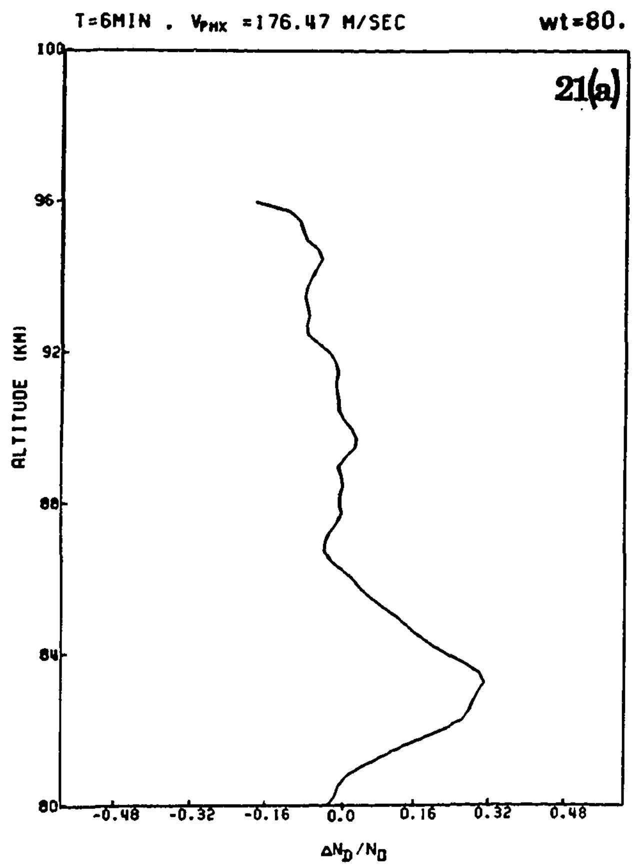
T=6MIN . V_PMX =176.47 M/SEC
wt=80.
21(a)
ALTITUDE (KM)
100
96
92
88
84
80
-0.48
-0.32
-0.16
0.0
0.16
0.32
0.48
ΔN_D/N_D

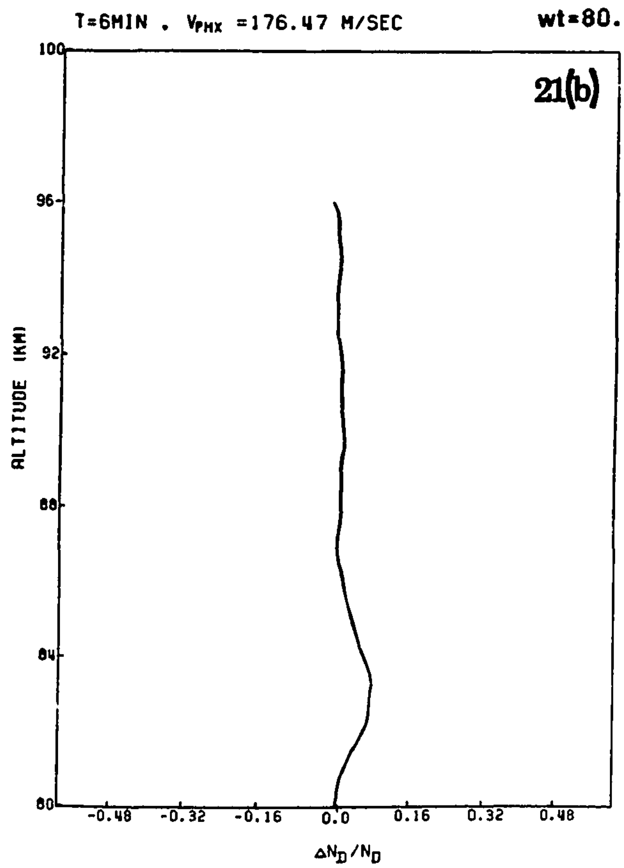
T=6MIN . V_PMX =176.47 M/SEC
wt=80.
21(b)
ALTITUDE (KM)
100
96
92
88
84
80
-0.48
-0.32
-0.16
0.0
0.16
0.32
0.48
ΔN_D/N_D

FIG. 22(a)

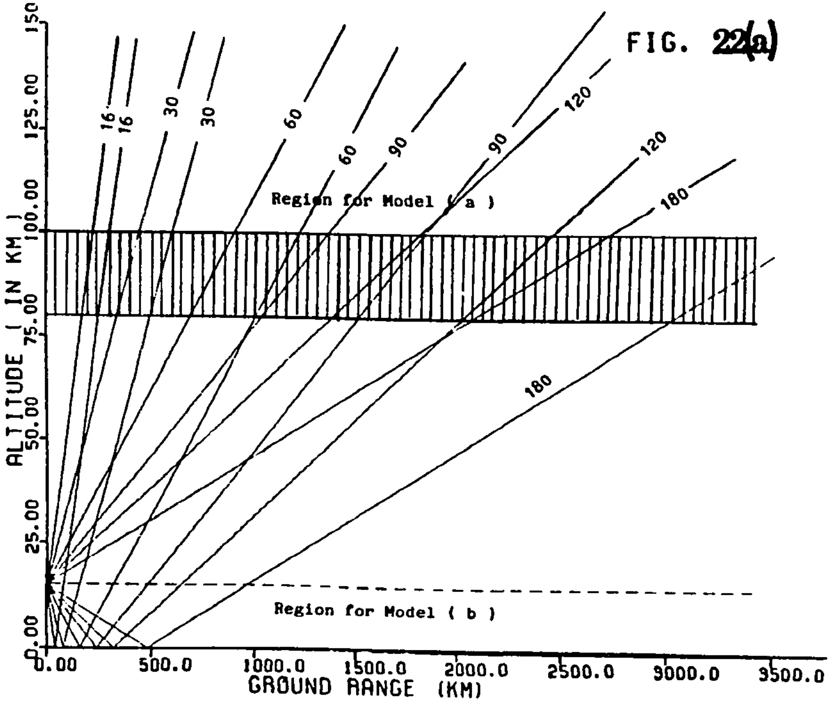

FIG. 22(b)

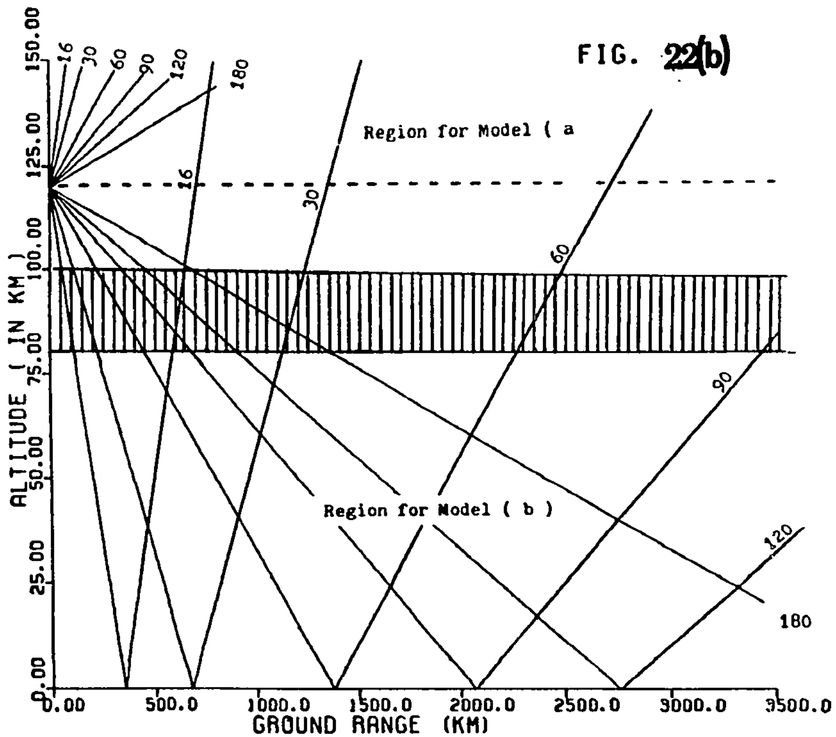

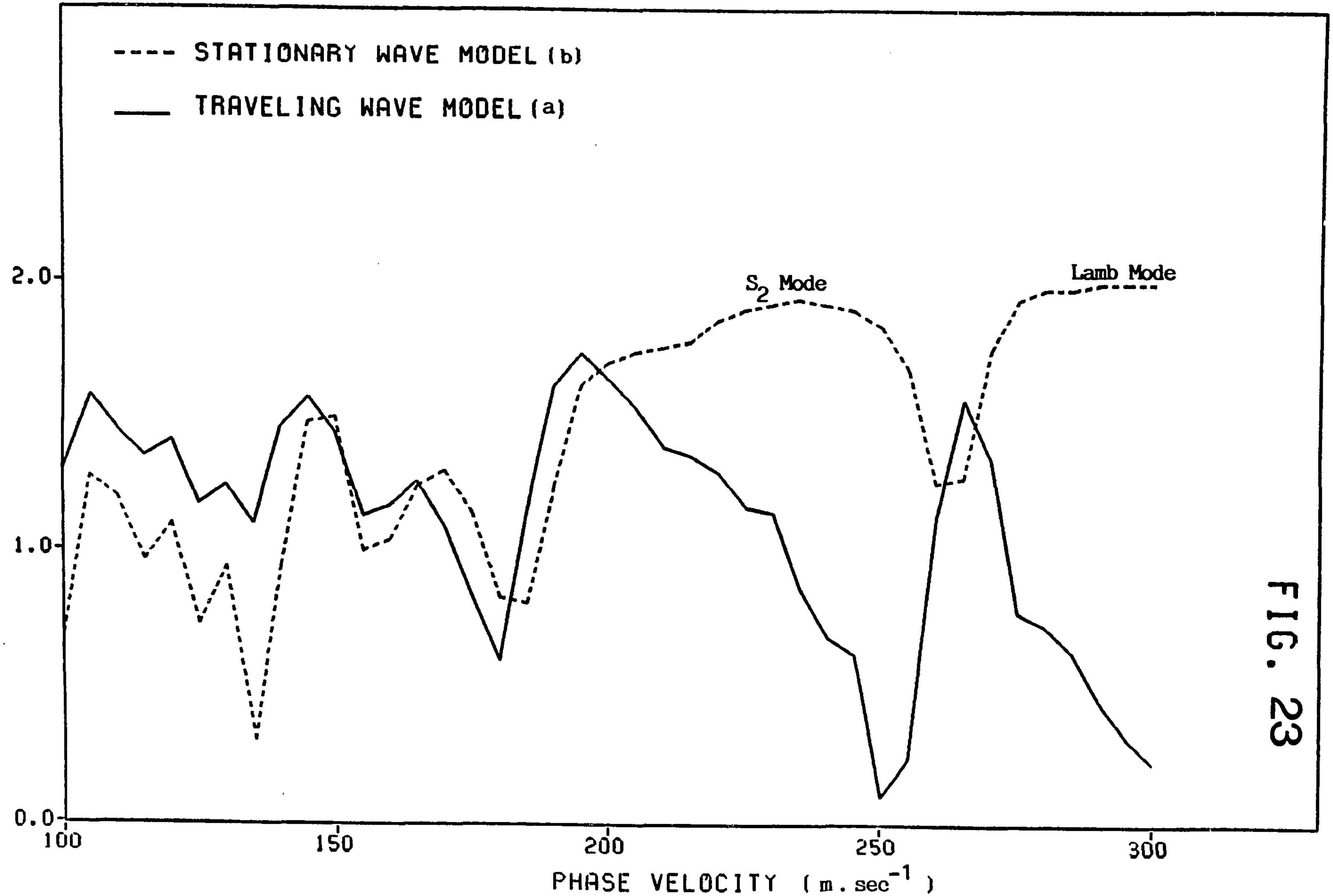
STATIONARY WAVE MODEL (b)
TRAVELING WAVE MODEL (a)
S2 Mode
Lamb Mode
2.0
1.0
0.0
100
150
200
250
300
PHASE VELOCITY (m. sec-1)

FIG. 23

Fig. 24

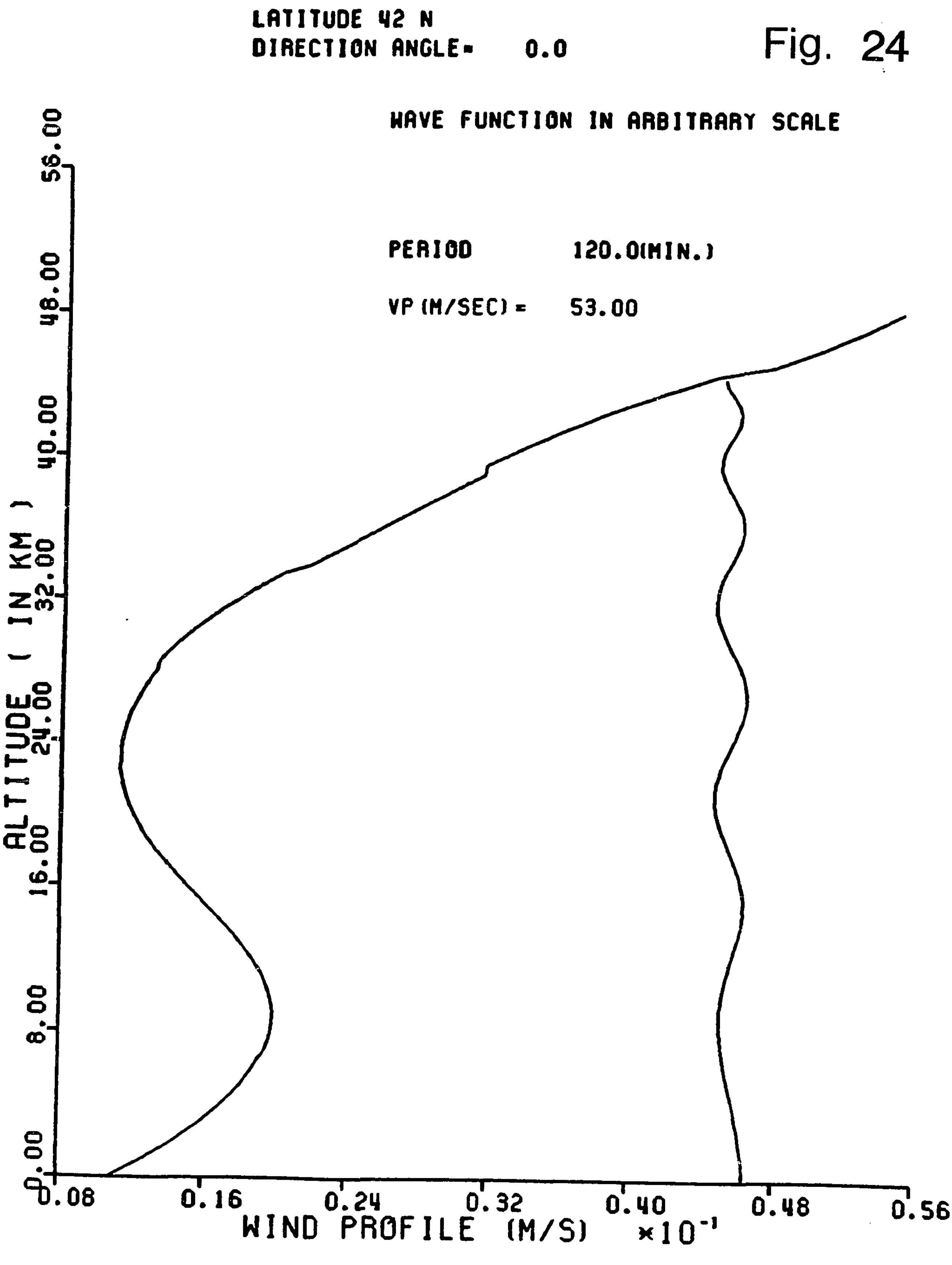
LATITUDE 42 N
DIRECTION ANGLE= 0.0
WAVE FUNCTION IN ARBITRARY SCALE
PERIOD 120.0(MIN.)
VP(M/SEC)= 53.00
ALTITUDE (IN KM)
0.00
8.00
16.00
24.00
32.00
40.00
48.00
56.00
0.08
0.16
0.24
0.32
0.40
0.48
0.56
WIND PROFILE (M/S) ×10⁻¹

Fig. 25

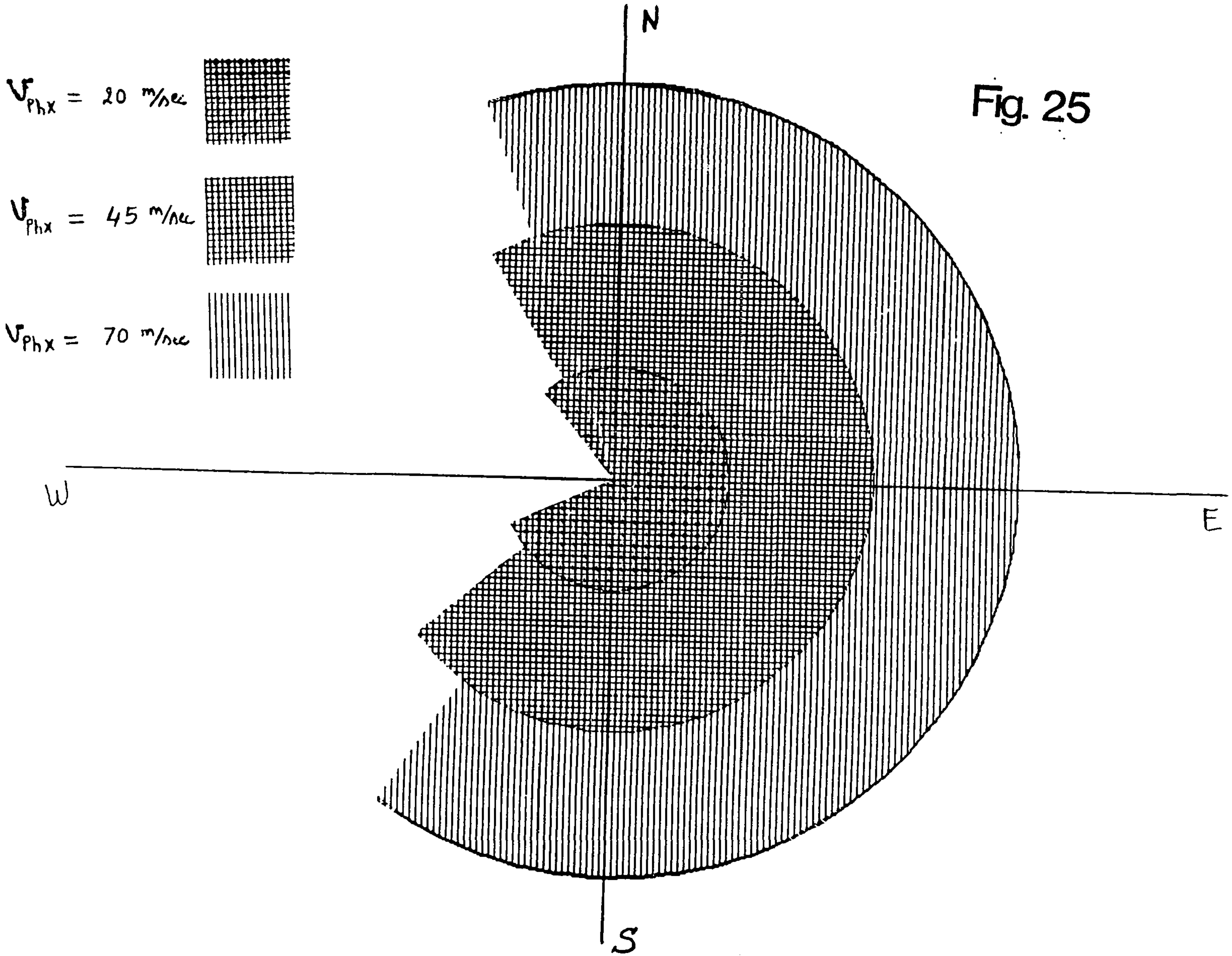

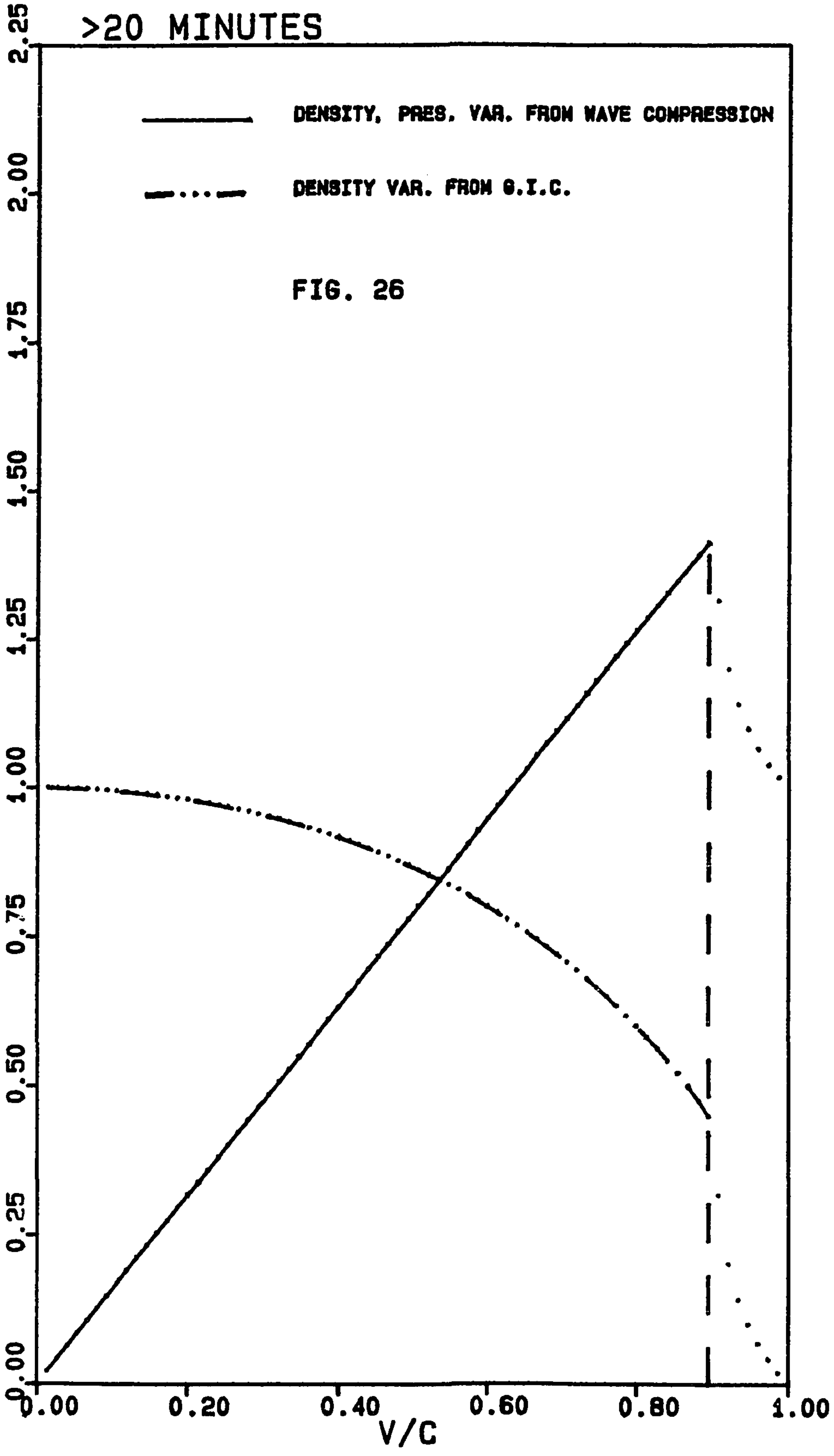

>20 MINUTES
DENSITY, PRES. VAR. FROM WAVE COMPRESSION
DENSITY VAR. FROM G.I.C.
FIG. 26
0.00
0.25
0.50
0.75
1.00
1.25
1.50
1.75
2.00
2.25
0.00
0.20
0.40
0.60
0.80
1.00
V/C

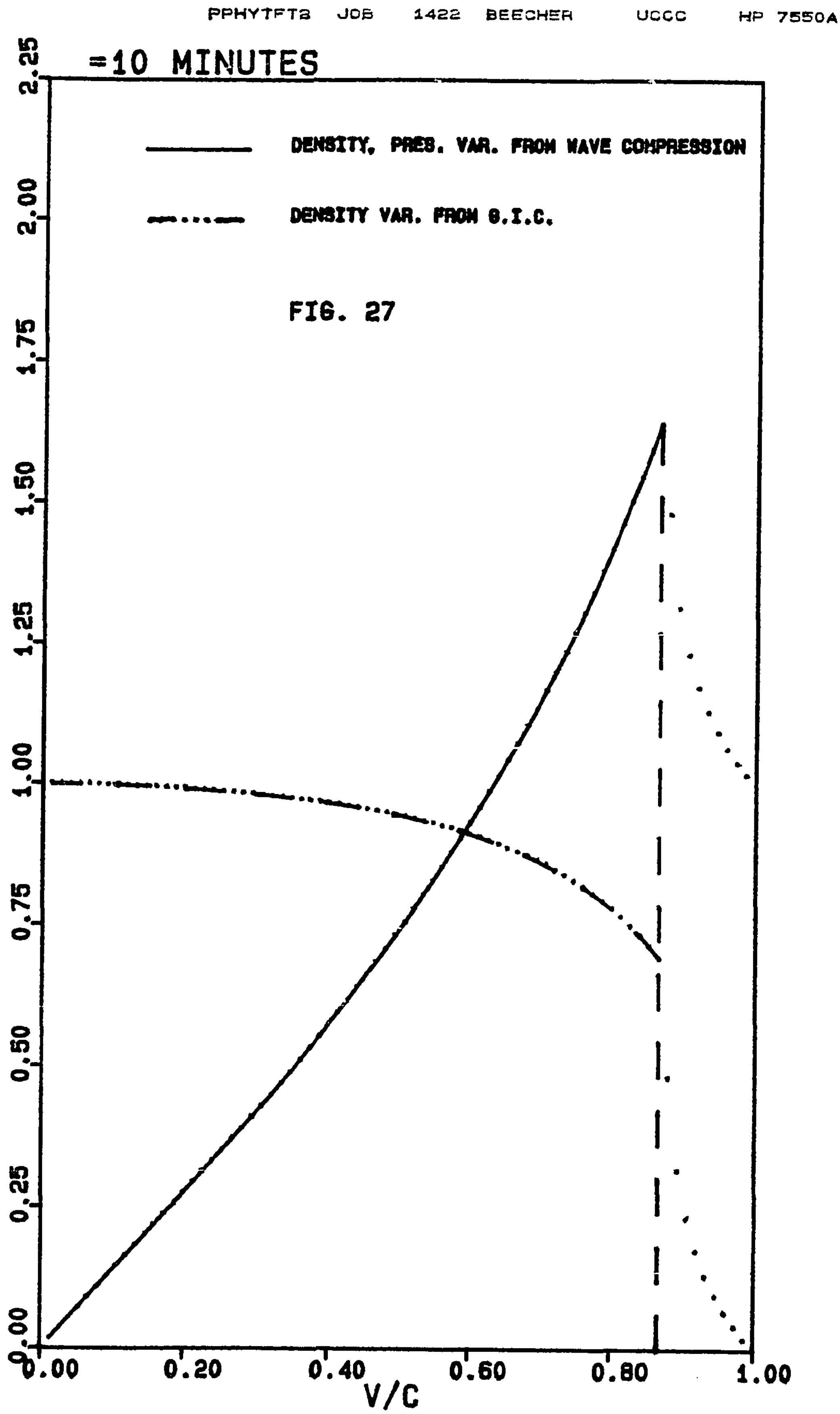
PPHYTFTB JOB 1422 BEECHER UCCC HP 7550A
=10 MINUTES
DENSITY, PRES. VAR. FROM WAVE COMPRESSION
DENSITY VAR. FROM G.I.C.
0.00
0.25
0.50
0.75
1.00
1.25
1.50
1.75
2.00
2.25
0.00
0.20
0.40
0.60
0.80
1.00
V/C

FIG. 27

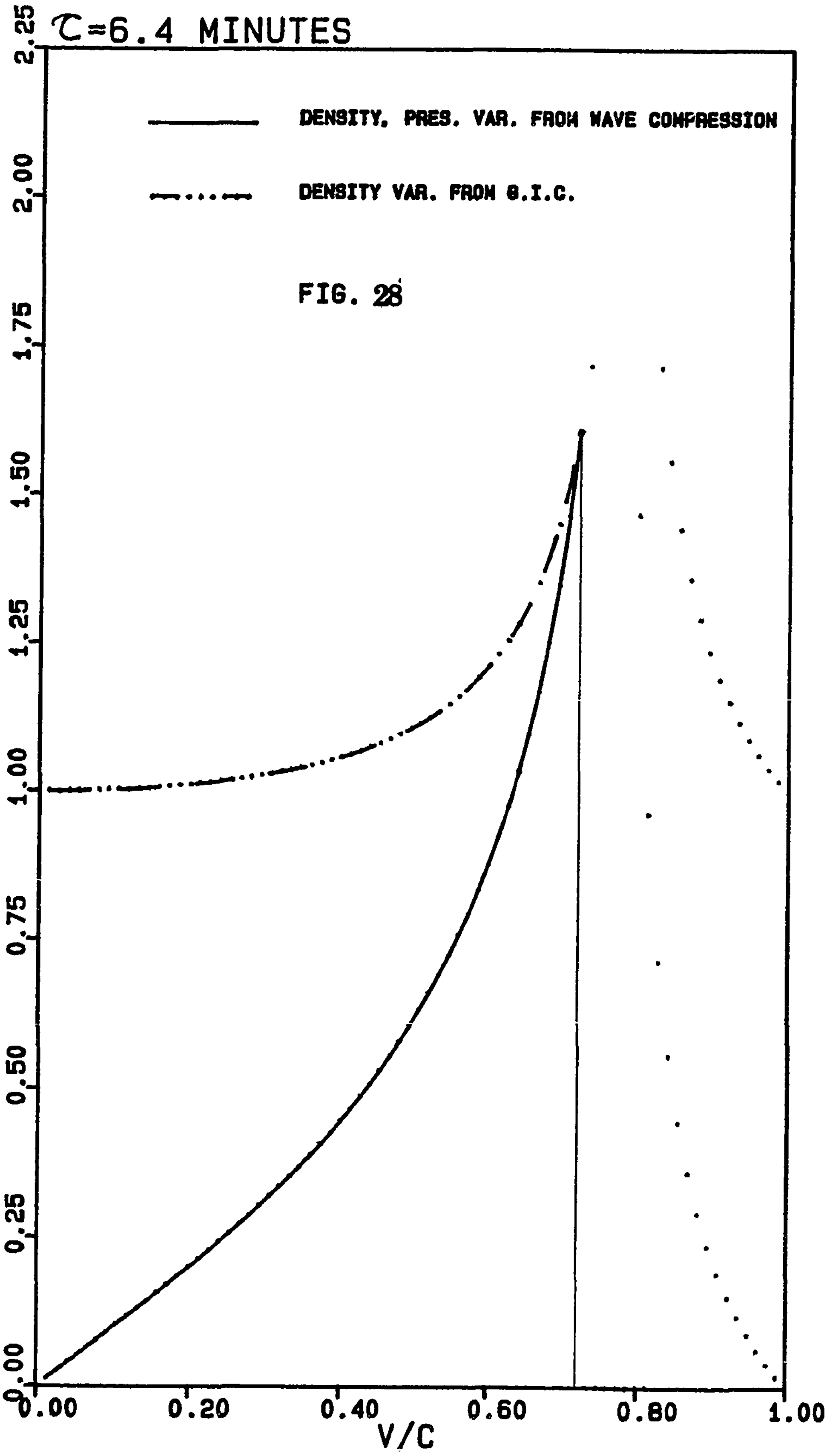
τ=6.4 MINUTES
DENSITY, PRES. VAR. FROM WAVE COMPRESSION
DENSITY VAR. FROM S.I.C.
0.00
0.25
0.50
0.75
1.00
1.25
1.50
1.75
2.00
2.25
0.00
0.20
0.40
0.60
0.80
1.00
V/C

FIG. 28

PPHYTFT2 JOB 1864 BEECHER UCCC HP 7550A

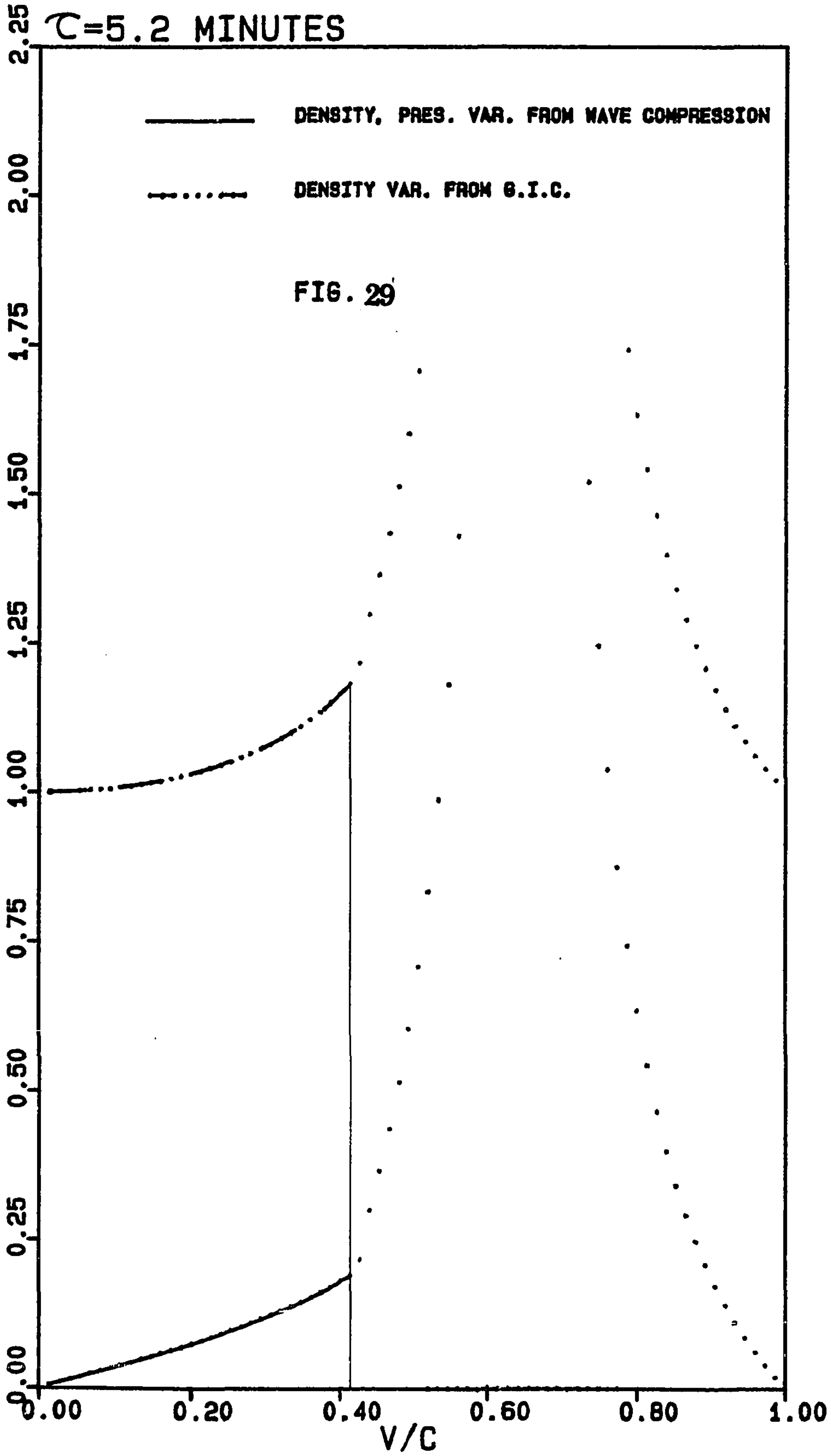

FIG. 29

PPHYTFT2 JOB 1901 BEECHER UCCC HP 7550A

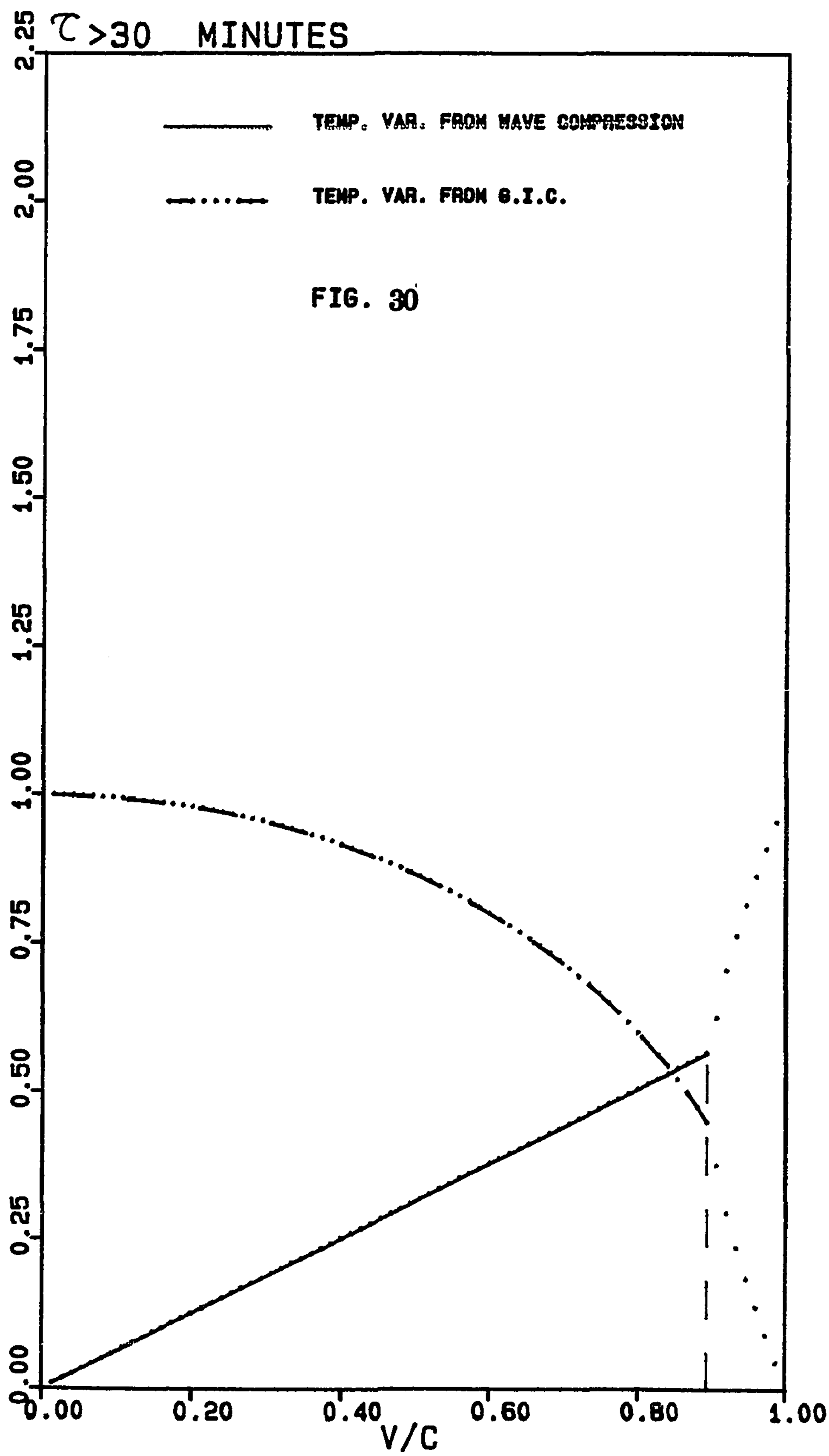

FIG. 30

PPHYTFT2 JOB 1915 BEECHER UCCC HP 7550A

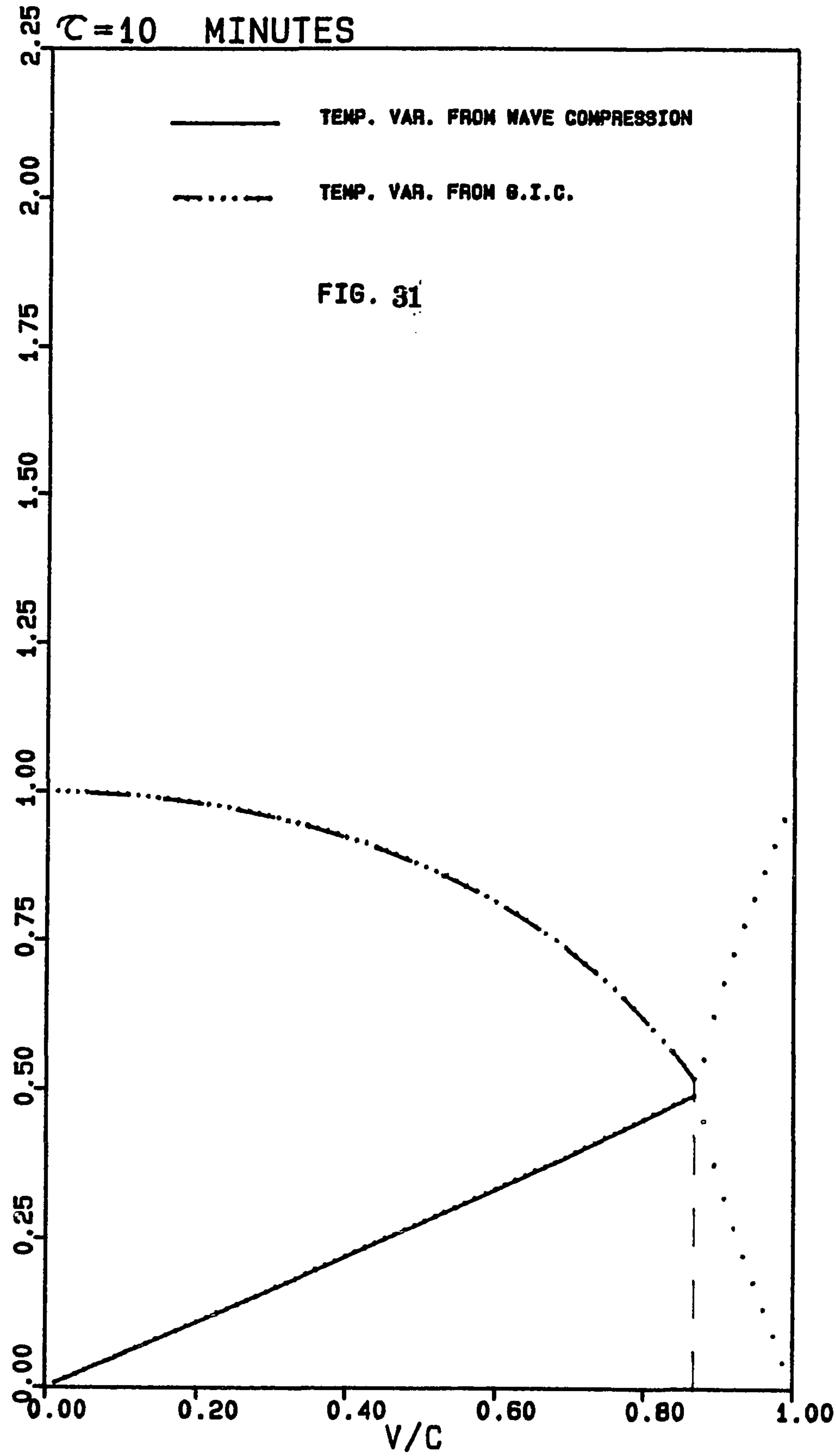

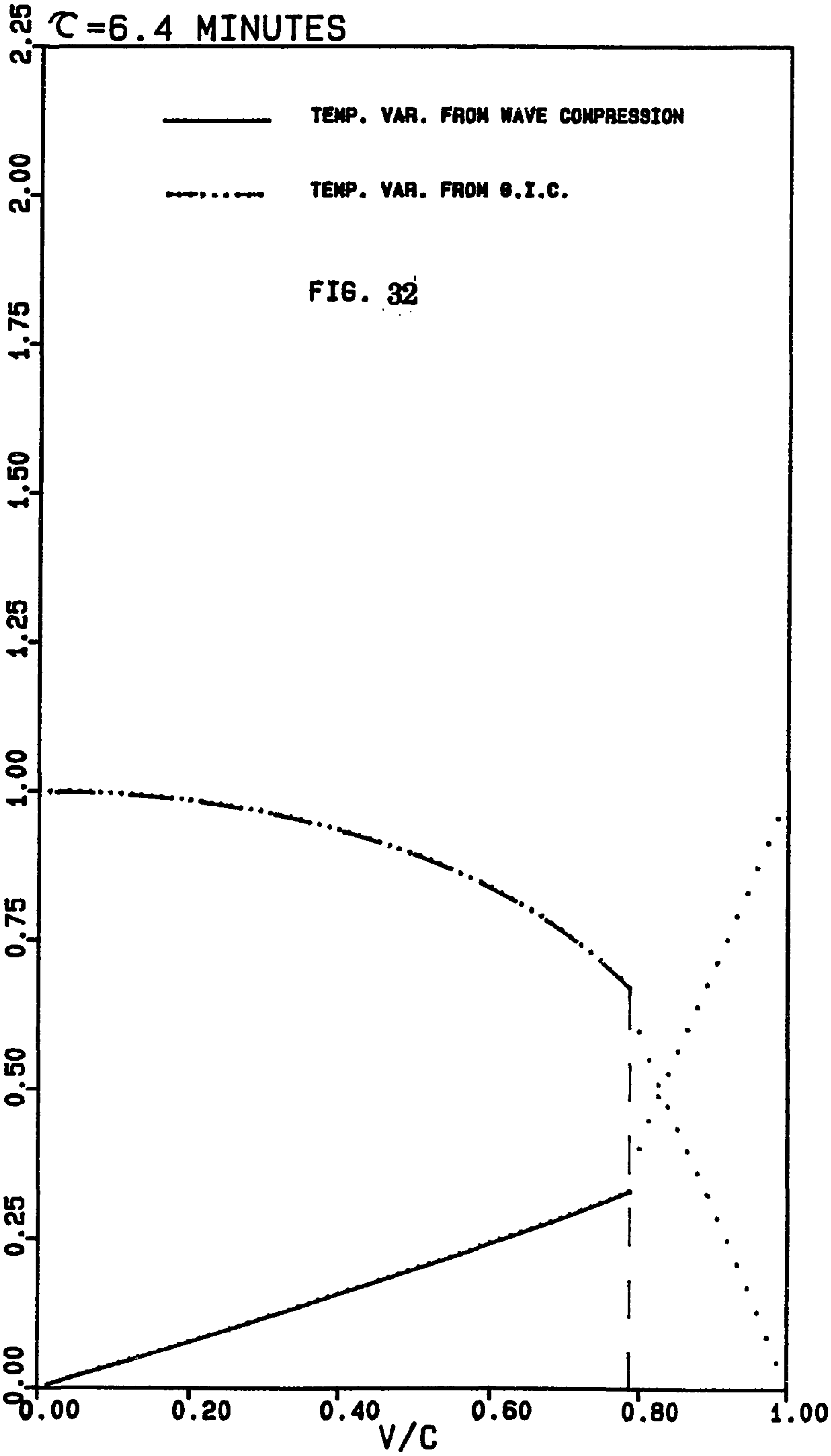
τ =6.4 MINUTES
TEMP. VAR. FROM WAVE COMPRESSION
TEMP. VAR. FROM G.I.C.
2.25
2.00
1.75
1.50
1.25
1.00
0.75
0.50
0.25
0.00
0.00
0.20
0.40
0.60
0.80
1.00
V/C

FIG. 32

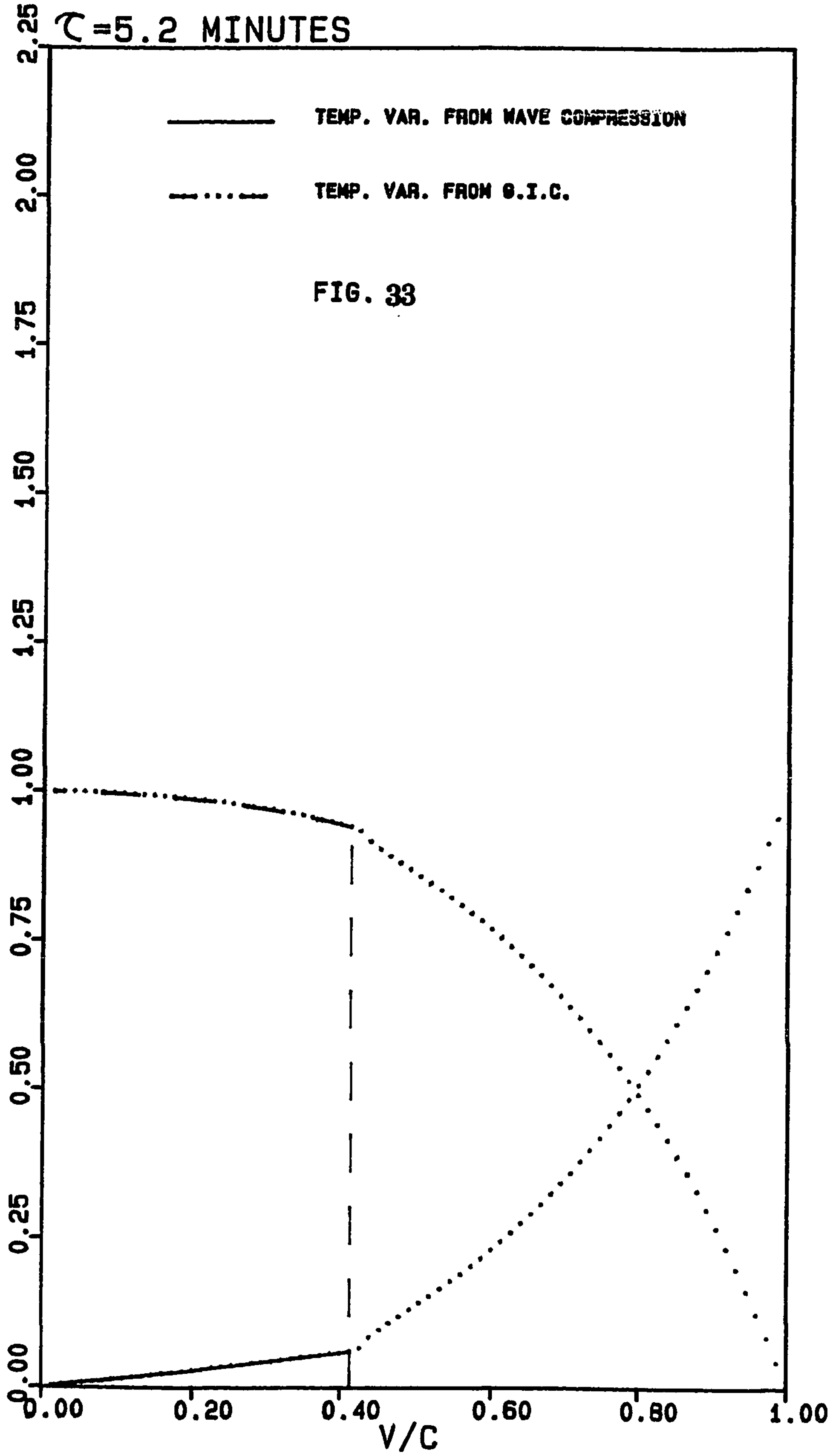
τ=5.2 MINUTES
TEMP. VAR. FROM WAVE COMPRESSION
TEMP. VAR. FROM S.I.C.
0.00
0.25
0.50
0.75
1.00
1.25
1.50
1.75
2.00
2.25
0.00
0.20
0.40
0.60
0.80
1.00
V/C

FIG. 33

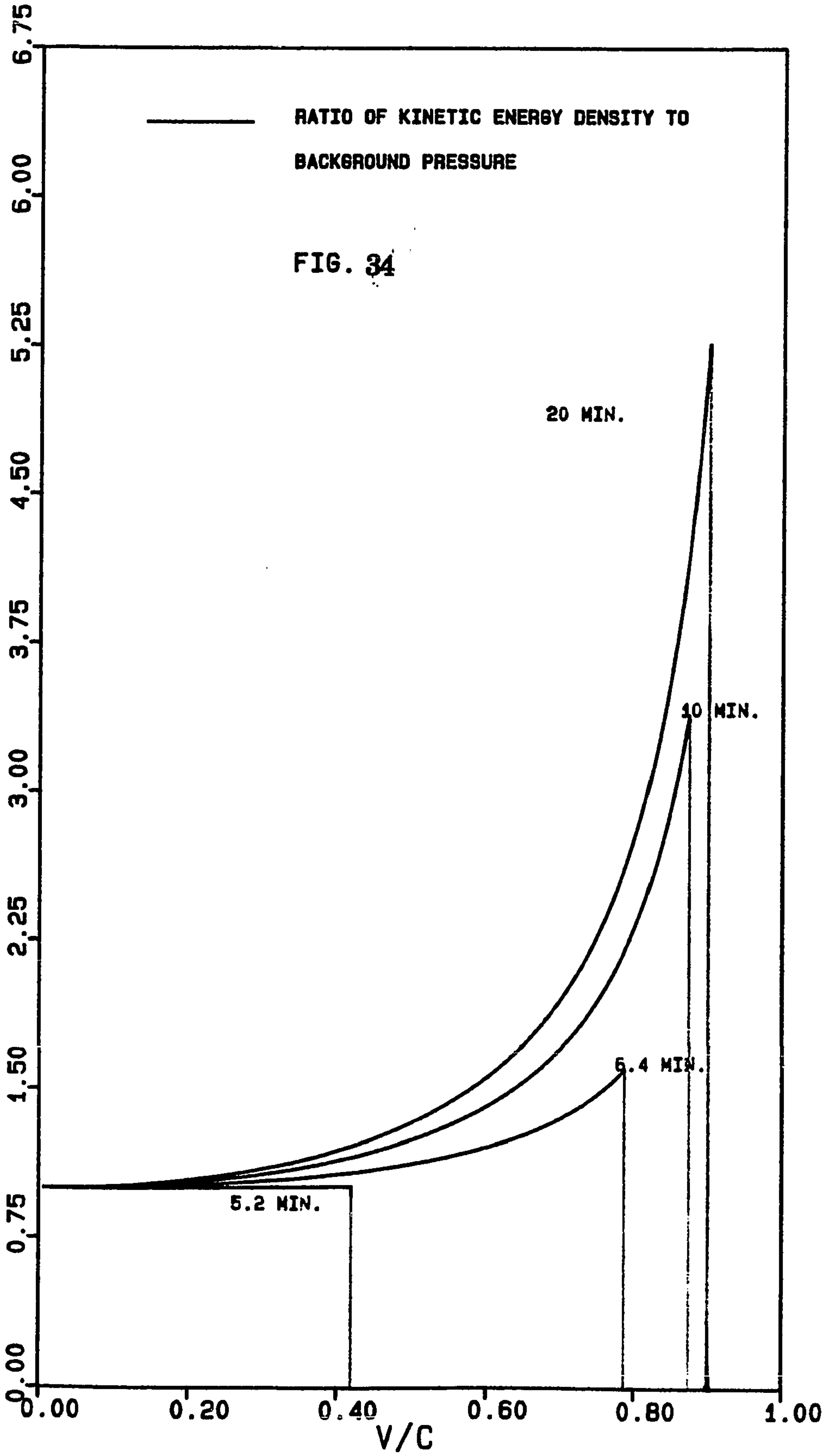

RATIO OF KINETIC ENERGY DENSITY TO BACKGROUND PRESSURE
20 MIN.
10 MIN.
6.4 MIN.
5.2 MIN.
0.00
0.75
1.50
2.25
3.00
3.75
4.50
5.25
6.00
6.75
0.00
0.20
0.40
0.60
0.80
1.00
V/C

FIG. 34